Preclinical evaluation of a COVID-19 vaccine candidate based on a recombinant RBD fusion heterodimer of SARS-CoV-2

Antonio Barreiro[1,11,*], Antoni Prenafeta[1,11,12,*], Gregori Bech-Sabat[1], Mercè Roca[1], Eva Perozo Mur[1], Ricard March[1], Luis González-González[1], Laia Madrenas[1], Júlia Corominas[1], Alex Fernández[1], Alexandra Moros[1], Manuel Cañete[1], Mercè Molas[1], Thais Pentinat-Pelegrin[1], Clara Panosa[1], Alberto Moreno[1], Ester Puigvert Molas[1], Eva Pol Vilarrassa[1], Jordi Palmada[1], Carme Garriga[1], Teresa Prat Cabañas[1], Javier Iglesias-Fernández[2], Júlia Vergara-Alert[3], Cristina Lorca-Oró[3], Núria Roca[3], Leira Fernández-Bastit[3], Jordi Rodon[3], Mònica Pérez[3], Joaquim Segalés[4,5], Edwards Pradenas[6], Silvia Marfil[6], Benjamin Trinité[6], Raquel Ortiz[6], Bonaventura Clotet[6,8], Julià Blanco[6,8], Jorge Díaz Pedroza[8], Rosa Ampudia Carrasco[8], Yaiza Rosales Salgado[8], Jordina Loubat-Casanovas[8], Sara Capdevila Larripa[8], Julia Garcia Prado[6,8], Jordi Barretina[8], Marta Sisteré-Oró[9], Paula Cebollada Rica[9], Andreas Meyerhans [9,10], Laura Ferrer[1]

[1]HIPRA. Avda. La Selva, 135, 17170 Amer (Girona), Spain.

[2]Nostrum Biodiscovery, Av. de Josep Tarradellas, 8-10, 3-2, 08029 Barcelona, Spain.

[3]Institut de Recerca i Tecnologia Agroalimentàries (IRTA), Centre de Recerca en Sanitat Animal (CReSA, IRTA-UAB), Campus de la UAB, 08193 Cerdanyola del Vallès, Spain.

[4]Universitat Autònoma de Barcelona, CReSA (IRTA-UAB), Campus de la UAB, 08193 Cerdanyola del Vallès, Spain.

[5]Departament de Sanitat i Anatomia Animals, Facultat de Veterinària, UAB, 08193 Cerdanyola del Vallès, Spain.

[6]IrsiCaixa. AIDS Research Institute, Germans Trias i Pujol Research Institute (IGTP), Can Ruti Campus, UAB, 08916 Badalona, Spain.

[7]University of Vic–Central University of Catalonia (UVic-UCC), 08500, Vic, Catalonia, Spain.

[8]Comparative Medicine and Bioimage Centre of Catalonia, Germans Trias i Pujol Research Institute (CMCiB-IGTP), 08916 Badalona, Spain.

[9]Infection Biology Laboratory, Department of Experimental and Health Sciences (DCEXS), Universitat Pompeu Fabra (UPF), 08003 Barcelona, Spain.

[10]Catalan Institution for Research and Advanced Studies (ICREA), Pg. Lluís Companys 23, 08010 Barcelona, Spain.

[11]These authors contributed equally.

[12]Lead contact: antoni.prenafeta@hipra.com

*Correspondence: antoni.prenafeta@hipra.com; antonio.barreiro@hipra.com

Summary: Current COVID-19 vaccines have been associated with a decline in infection rates, prevention of severe disease and a decrease in mortality rates. However, SARS-CoV-2 variants are continuously evolving, and development of new accessible COVID-19 vaccines is essential to mitigate the pandemic. Here, we present data on preclinical studies in mice of a receptor-binding domain (RBD)-based recombinant protein vaccine (PHH-1V) consisting of an RBD fusion heterodimer comprising the B.1.351 and B.1.1.7 SARS-CoV-2 variants formulated in SQBA adjuvant, an oil-in-water emulsion. A prime-boost immunisation with PHH-1V in BALB/c and K18-hACE2 mice induced a $CD4^+$ and $CD8^+$ T cell response and RBD-binding antibodies with neutralising activity against several variants, and also showed a good tolerability profile. Significantly, RBD fusion heterodimer vaccination conferred 100% efficacy, preventing mortality in SARS-CoV-2 infected K18-hACE2 mice, but also reducing Beta, Delta and Omicron infection in lower respiratory airways. These findings demonstrate the feasibility of this recombinant vaccine strategy.

Keywords: SARS-CoV-2, COVID-19, second-generation vaccines, RBD fusion heterodimer, preclinical, mice.

1. Introduction

In December 2019, severe acute respiratory syndrome coronavirus 2 (SARS-CoV-2) was identified as the etiological agent of the coronavirus disease 2019 (COVID-19). Soon afterwards, the scientific community and the pharmaceutical industry began focusing on the development of effective COVID-19 vaccines to mitigate the health emergency. Thanks to these efforts, several vaccines are currently available, and more than 12.9 billion doses have been administered worldwide (November 2022)[1]. The decline in new infection rates in many countries coincides with the introduction of vaccines. However, COVID-19 cases continue to emerge, probably due to the appearance and evolution of SARS-CoV-2 variants, the decline of immunological protection provided by the current vaccines, and especially the lack of homogenous distribution of COVID-19 vaccines, with only 22.5% of people in low-income

57 countries having received at least one dose (December 2021)[2,3]. As the global outbreak
58 continues, the pandemic is far from being over and it is not clear if the available vaccines will
59 be sufficient to revert the situation. Thus, it is still critical to develop second-generation
60 vaccines using different platforms that are effective against new variants and that could be
61 further used as a booster, particularly to maintain or even enhance immunity against SARS-
62 CoV-2[4,5]. Moreover, it is of relevance that these recent vaccines can be stored in refrigerated
63 conditions, making them easier to distribute and avoiding more expensive and less available
64 ultra-low temperature storage and transport conditions to ensure their global supply.
65 Currently authorised vaccines, whether approved under emergency use or fully licensed, are
66 based on viral vectors, inactivated viruses, nucleic acid-based vaccines, and protein subunit
67 vaccines[6].
68 SARS-CoV-2 is a betacoronavirus belonging to the subfamily *Coronovirinae,* within the family
69 *Coronaviridae* and the order *Nidovirales*. The SARS-CoV-2 genome is a positive-sense single-
70 stranded RNA (+ssRNA) molecule. The genome size ranges between 27 and 32 kbp, one of the
71 largest known RNA viruses. The genomic structure of SARS-CoV-2 contains at least six open
72 reading frames (ORFs), encoding for at least four structural proteins, namely: envelope or spike
73 (S) glycoprotein; membrane (M) proteins, responsible for the shaping of the virions; envelope
74 (E) proteins, responsible for the virions assembly and release; and nucleocapsid (N) proteins,
75 involved in the RNA genome packaging[7]. The trimeric S glycoprotein of SARS-CoV-2 is the
76 primary target of viral neutralising antibodies and has been the main protein candidate for
77 vaccine development[8]. Consistent with SARS-CoV, angiotensin-converting enzyme 2 (ACE2)
78 binding of the S protein allows cellular entry of SARS-CoV-2 viral particles[9]. This protein
79 consists of 2 domains, S1 and S2, allowing the binding of the viral particles and cellular entry by
80 fusing with the host cell membrane[10]. The receptor-binding domain (RBD) (Thr333-Gly526) is
81 found in the S1 domain and it contains a highly immunogenic receptor-binding motif (RBM)
82 that directly interacts with ACE2 and neutralising antibodies[11]. Therefore, most key mutations

83 are found in the RBM, allowing the virus to adapt and escape the previously developed
84 immunity[12,13]. To date, several SARS-CoV-2 VoCs with key mutations in the S protein have
85 emerged: Alpha (B.1.1.7), Beta (B.1.351), Gamma (P.1), Delta (B.1.617.2) and Omicron
86 (B.1.1.529)[14,15].

87 The S protein is the primary target in vaccine development against betacoronaviruses due to
88 its accessibility for immune recognition[16]. It has been reported that two proline substitutions in
89 the original S protein sequence (S-2P) of MERS-CoV, SARS-CoV and HKU1 coronavirus maintain
90 the antigenic conformation but retain S proteins in the prototypical prefusion conformation[17].
91 Thus, learning from these previous results, this S-2P design is used in the licensed mRNA-based
92 vaccines Comirnaty® (Pfizer-BioNTech)[18] and Spikevax® (Moderna)[19], which substitute the K986
93 and V987 residues for prolines from the original S protein variant. Likewise, the adenoviral
94 vector-based vaccine Jcovden® (Johnson & Johnson) also contains DNA-encoding for the S-2P
95 protein of SARS-CoV-2[20].

96 Adjuvanted protein-based subunit vaccines represent an important type of vaccine, yet their
97 development has lagged compared to other platforms due to the need to optimise the
98 manufacturing process for each protein antigen. The most advanced subunit vaccine
99 programme against COVID-19 is the Novavax vaccine (NVX-CoV-2373, marketed as
100 Nuvaxovid®), which is produced in insect cells in combination with a saponin-based adjuvant
101 (Matrix-M)[21]. This vaccine consists of the stable full-length S protein in the antigenically
102 optimal prefusion conformation. In addition, the Sanofi-GSK vaccine, known as VidPrevtyn
103 Beta®, consists of soluble prefusion-stabilised S trimers from SARS-CoV-2 produced in insect
104 cells combined with the AS03 adjuvant[22]. Both vaccines have been tested in human clinical
105 trials and have recently received an EU marketing authorisation[21,23]. Notably, recombinant
106 proteins are competitive vaccine candidates with an adequate safety profile, no risk of genome
107 integration, no live components, and suitable for people with compromised immune
108 systems[24], showing high productivity yields and good stability profiles[24-26].

109 Most cloned neutralising antibodies target the RBD in the S1 domain[27], although there are
110 additional immunogenic epitopes outside this domain[28]. It has been reported that more than
111 90% of neutralising antibodies isolated from convalescent patients target the RBD in one-third
112 of cases[29]. Moreover, depleted sera and plasma samples from individuals vaccinated with a
113 250-µg dose of the mRNA-1273 vaccine showed that up to 99% of neutralising antibodies
114 target the RBD, even though the antigen is based on the whole prefusion spike conformation[30].
115 Given that the RBD domain of the S protein directly interacts with the ACE2 receptor, RBD-
116 targeting antibodies are not expected to cause antibody-dependent enhancement (ADE),
117 unlike non-neutralising or sub-neutralising antibodies[31], highlighting the importance of the
118 RBD in the immune response against SARS-CoV-2 and emphasising its relevance as a powerful
119 and efficient immunogen in vaccine design.
120 In view of the inherent particularities of the S protein, and especially the RBD domain, our
121 team developed a vaccine-candidate platform based on this immunogen. From amongst the
122 tested preliminary vaccine candidates, combined with one or several adjuvants, we finally
123 proceeded with a protein-based subunit vaccine candidate, namely PHH-1V, consisting of a
124 recombinant RBD fusion heterodimer of the B.1.351 and B.1.1.7 variants of SARS-CoV-2
125 expressed in Chinese hamster ovary (CHO) cells and formulated with the squalene-based
126 adjuvant (SQBA). Specifically, the SQBA adjuvant is an oil-in-water emulsion comprising well-
127 known components which are used as adjuvants in human medicine[32]. Hence, the main aims
128 of this study were to assess the safety and efficacy of the PHH-1V vaccine in BALB/c and K18-
129 hACE2-transgenic mice models, and to characterise the RBD fusion heterodimer antigen and
130 its immunogenicity.

131 **2. Results**

132 **2.1. Recombinant RBD fusion heterodimer expression and characterisation**

133 The antigen of the PHH-1V vaccine candidate is a recombinant RBD fusion heterodimer based
134 on the B.1.351 (Beta) and B.1.1.7 (Alpha) SARS-CoV-2 variants (**Figure 1A**). The N-terminal

135 monomer contains the amino acid sequence of the SARS-CoV-2 RBD protein from the B.1.351
136 variant, whereas the C-terminal monomer contains the amino acid sequence of the SARS-CoV-
137 2 RBD protein from the B.1.1.7 variant. The rationale behind this antigenic construct was based
138 on maximisation of the affinity constant towards its target receptor, allowing the
139 accommodation of each RBD variant bound to a single hACE monomer within the same or a
140 different receptor. Three-dimensional structural models generated with AlphaFold2[33]
141 highlighted the coexistence of two different conformations of the PHH-1V construct. More
142 specifically, one of the conformations is characterised by a protein-protein interaction
143 between both RBD variants, whereas the other presents separated RBD domains stabilised by
144 interactions of the N-/C-terminal regions (**Figure 2B**). RBD monomer binding towards
145 individual human ACE2 (hACE2) units requires the preferential adoption of a separated RBD
146 stabilised conformation, and thus construct generation followed this requirement.
147 The protein-protein interaction energies of two construct variant candidates, B.1.351-B.1.1.7
148 and B.1.1.7-B.1.351, were estimated by means of molecular mechanics-generalised Born
149 surface area (MM-GBSA) calculations. MM-GBSA results highlighted the B.1.351-B.1.1.7 variant
150 as the preferred construct candidate with a protein-protein interaction energy of -78.23
151 $kcal \cdot mol^{-1}$ as compared to the value of -98.06 $kcal \cdot mol^{-1}$ for the inverse construct. This suggests
152 that the N-/C-terminal stabilised conformation is energetically more favourable in the B.1.351-
153 B.1.1.7 construct than in the B.1.1.7-B.1.351 construct. The interaction energies of both
154 studied constructs, in a stabilised N-/C-terminal conformation, and the hACE2 receptor were
155 also computed by means of MM-GBSA simulations (**Figure 2B**). Although both models showed
156 similar binding affinities to hACE2, the Beta N-terminus plus Alpha C-terminus configuration
157 clearly exposed those mutations involved in the higher affinity towards the human ACE2
158 receptor on the protein surface and the potential immune evasion by both variants. Hence, the
159 selection of the B.1.351-B.1.1.7 fusion heterodimer as the PHH-1V vaccine antigen was based

160 on the lower free energy required for the formation of the stabilised N-/C-terminal
161 conformation.
162 The heterodimer is expressed in mammalian CHO cells and is formulated with the SQBA
163 adjuvant. After expressing the antigen in a bioreactor fed-batch cultivation, it is purified by a
164 downstream process consisting of sequential stages, including depth and tangential filtration,
165 chromatography steps, and sterile filtrations. The final product is a highly purified antigen, as
166 determined by SDS-PAGE (**Figure 1C**) and SEC-HPLC (**Figure 1D**), suitable for vaccine
167 formulation. Moreover, surface plasmon resonance (SPR) analysis showed an affinity constant
168 of 0.099 nM for hACE2 (**Figure 1E**).

169 **2.2. Recombinant RBD fusion heterodimer antigen immunogenicity in BALB/c mice**

170 *2.2.1. RBD-specific binding and neutralising antibody titres upon PHH-1V vaccination*

171 BALB/c mice (Environ, IN, USA) were immunised with different doses of the recombinant RBD
172 fusion heterodimer antigen (group B: 0.04 µg, group C: 0.2 µg, group D: 1 µg, group E: 5 µg;
173 and group F: 20 µg) on days (D) 0 and 21. Mice were also immunised with PBS as a control
174 group (group A). A schematic view of the immunisation protocol is depicted in **Figure 2**.
175 The prime immunisation of BALB/c mice with the PHH-1V candidate induced higher titres of
176 RBD binding antibodies in groups C to F compared to the control (group A, immunised with
177 PBS) on day 21 post-first immunisation (D21) ($p<0.01$) (**Figure 3A**). After the prime-boost
178 immunisation, all vaccinated groups (B to F) reached higher IgG titres than the control group
179 on D35/D37 (14/16 days after the boost; $p<0.01$). On D35/D37, specific SARS-CoV-2 RBD-
180 binding antibodies were detected in groups B to D in a dose-dependent manner, with
181 significant differences between these groups ($p<0.01$). However, no significant differences
182 were observed between the groups immunised with more than 1 µg of recombinant RBD
183 fusion heterodimer antigen (groups D to F). Therefore, the IgG response was saturated from 1-
184 µg immunisation. Likewise, the IgG2a/IgG1 ratios were calculated as a surrogate of the
185 Th1/Th2 cellular immune response to estimate the type of cellular immune response elicited

186 by the vaccine. The IgG2a/IgG1 ratio of groups E and F was 0.74 and 0.75, respectively, which
187 suggests a balanced Th1/Th2 immunogenic response upon PHH-1V vaccination in mice (**Figure**
188 **3B**).
189 SARS-CoV-2 neutralising antibodies titres in sera from BALB/c mice were determined by a
190 pseudovirus-based neutralisation assay (PBNA) against the S protein of different variants on
191 D35/D37 (14/16 days after the boost). Prime-boost immunisation of groups C to F induced
192 higher neutralising antibody titres against the S protein of the Alpha variant compared to the
193 control group A (*p<0.01*) (**Figure 3C**). No neutralising antibody response was observed in group
194 B, although IgG binding antibodies were detected on D35/D37. The mean neutralising antibody
195 titres observed in groups C and D remained the same since no statistically significant
196 differences were observed. However, vaccination with 5 µg (group E) and 20 µg (group F) of
197 RBD fusion heterodimer antigen induced higher neutralising titres than group C and groups C
198 and D, respectively. Interestingly, high neutralising titres against all the tested variants (Alpha,
199 Beta, Delta and Omicron BA.1) were detected in sera from group F compared to control group
200 A (*p<0.01*) (**Figure 3D**).
201 *2.2.2. RBD-specific cellular immune response upon PHH-1V vaccination*
202 The characterisation of the antigen-specific response of splenic T cells 14/16 days after the
203 boost immunisation was performed by intracellular cytokine staining (ICS) and enzyme-linked
204 immunospot (ELISpot) assays in female BALB/c mice from groups A (control), E and F
205 (vaccinated with 5 µg or 20 µg of recombinant protein RBD fusion heterodimer, respectively).
206 The ICS data indicate that upon stimulation with an RBD peptide pool, splenocytes from group
207 F displayed significant activation of $CD4^+$ T cells expressing IFN-γ (*p<0.01*), IL-2 (*p<0.05*) and
208 Th1-like cytokines (IFN-γ and/or TNF-α and/or IL-2; *p<0.05*) compared to the control group
209 (**Figure 4A**). No significant antigen-specific response of $CD4^+$ T cells expressing TNF-α or IL-4
210 was observed in group F when compared to the control group. Notably, immunisation of mice
211 with a lower RBD dose (group E) did not induce $CD4^+$ T cells secreting IFN-γ, TNF-α, IL-2 and/or

212 IL-4 after the *in vitro* restimulation. Furthermore, splenocytes from group F showed activation
213 of $CD8^+$ T cells expressing IFN-γ (*0.05<p<0.1*) and IL-2 (*p<0.05*) after the antigen-specific
214 restimulation compared to the control group (**Figure 4B**). Likewise, splenocytes from group F
215 also elicited significantly higher $CD8^+$ T cells expressing IFN-γ (*p<0.05*) and IL-2 (*p<0.01*)
216 compared to the group E. No $CD8^+$ T cell response was observed in splenocytes from group E
217 compared to the control group.
218 The IFN-γ and IL-4 ELISpot assays showed no significant differences between the two doses of
219 recombinant protein RBD fusion heterodimer (group E vs group F) (**Figure 4C**). However, both
220 groups showed a higher percentage of IFN-γ^+ and IL-4^+ spots compared to the control group
221 (*p<0.01*). Importantly, the percentage of IFN-γ^+ and IL-4^+ in group F was similar, denoting a
222 balanced Th1/Th2 response, while the percentage of IL-4^+ spots was significantly higher than
223 IFN-γ^+ spots in group E (*p<0.01*), suggesting a Th2-biased response in mice immunised with 5
224 µg of recombinant protein RBD fusion heterodimer.
225 Extracellular cytokine levels were measured by Luminex Multiplex in supernatants from
226 splenocytes stimulated with a pool of peptides from SARS-CoV-2 RBD. The levels of IL-2
227 (*p<0.05*) and IL-5 (*p<0.01*) were higher in the supernatants from group E splenocytes compared
228 to the control group (**Figure 4D**). Similarly, the levels of IL-5 (*p<0.01*) and TNF-α (*p<0.05*) were
229 statistically higher in group F compared to group A. A tendency towards an increase in the
230 levels of IL-2 (*0.05<p<0.1*) was also observed in group F compared to group A.

231 **2.3. Recombinant RBD fusion heterodimer antigen immunogenicity and efficacy against**
232 **SARS-CoV-2 Wuhan/D614G in K18-hACE2 mice**

233 To analyse the immunogenicity and protective efficacy of the PHH-1V vaccine candidate
234 against COVID-19 and the pathogenic outcomes derived from the SARS-CoV-2 infection, the
235 mouse strain B6.Cg-Tg(K18-ACE2)2Prlmn/J (K18-hACE2) (Jackson Laboratories, ME, USA) was
236 used as a challenge model. Groups were vaccinated intramuscularly with PBS (groups A and B),
237 10 µg of PHH-1V (group C) or 20 µg of PHH-1V (group D) following the two-dose prime-and-

238 boost schedule: 1st dose (prime) on D0 and 2nd dose (boost) on D21 (**Figure 2**). The SARS-CoV-2
239 (Wuhan/D614G strain) challenge was performed on group B-D animals on D35 through
240 intranasal instillation.

241 The primary endpoint for reporting the protective capacity of the vaccine candidates was
242 weight loss and/or mortality post-challenge. Clinical signs and survival are presented in **Figure**
243 **5A**. Clinical signs of the SARS-CoV-2 infection were observed only in the non-vaccinated and
244 infected group (B) on days 5 (3 animals) and 6 (3 animals) post-challenge. In all cases, clinical
245 signs led to endpoint criteria and the animals were euthanised. Thus, survival of group B was
246 significantly different than the other groups (*p<0.01*). The daily individual bodyweights of each
247 group during the vaccination period and post-challenge are shown in **Figures S1 B** and **5B**,
248 respectively. The animals from group B experienced remarkable weight loss from D3 post-
249 challenge onwards, as expected due to the SARS-CoV-2 infection, showing a significantly lower
250 weight compared to vaccinated animals from groups C and D on D5 and 6 post-challenge
251 (*p<0.01*).

252 SARS-CoV-2 neutralising antibodies against the original Wuhan/D614G strain were also
253 analysed in SARS-CoV-2 infected K18-hACE2 mice upon vaccination to study the
254 immunogenicity of PHH-1V vaccine in a humanised mice model (**Figure S2 A**). Animals from
255 group D elicited significant higher SARS-CoV-2-specifc neutralising titres 0-, 2- and 4-days post-
256 infection (dpi) (*p<0.01*) and 7-8 dpi (*p<0.05*) compared to group B. Animals from group C
257 elicited higher specific neutralising titres 0, 2 (*p<0.01*), 4 dpi (*p<0.05*) and 7-8 dpi (*p<0.01*) *vs.*
258 control group (B). Furthermore, the levels of neutralising antibodies were similar between
259 both vaccinated groups.

260 Total viral RNA was determined in the lungs, nasal turbinate, oropharyngeal swabs and brain
261 (**Figure 5C**), but also in trachea, heart, pharynx and spleen (**Figure S3**). Viral RNA was
262 determined by real-time quantitative polymerase chain reaction (RT-qPCR) on D37 (2 dpi), D39
263 (4 dpi), D42 (in males, 7 dpi) and D43 (in females, 8 dpi), or at the time of euthanasia in

264 animals reaching endpoint criteria before the scheduled euthanasia day. Immunisation with 10
265 µg of PHH-1V (group C) reduced the viral load measured by PCR in the lungs on all dpi studied
266 (*p<0.01*), in nasal turbinate on all dpi studied (*p<0.05*), in oropharyngeal swabs 2 dpi (*p<0.05)*
267 and 7-8 dpi (*p<0.01*), and in brain 4 and 7-8 dpi (*p<0.01*) compared to the infected control
268 (group B). Vaccination with 20 µg of PHH-1V (group D) also reduced the viral load measured by
269 PCR in the lungs on all dpi studied (*p<0.01*), in nasal turbinate on all dpi studied (*p<0.01*), in
270 oropharyngeal swabs 7-8 dpi (*p<0.01*), and in brain 4 and 7-8 dpi (*p<0.01*) compared to group B
271 (**Figure 5C**). Likewise, both vaccinated groups reduced significantly viral RNA in the trachea
272 (*p<0.01*), pharynx (*p<0.05)* and spleen (*p<0.01*) compared to control group (**Figure S3**). In
273 heart, there was a tendency towards a decrease in both vaccinated groups 4 dpi compared to
274 group B.
275 Virus titres were determined using a standard 50% tissue culture infectious dose ($TCID_{50}$) assay
276 on positive samples of RT-qPCR in lungs, nasal turbinates, oropharyngeal swabs and brain
277 (**Figure 5D**). Samples from groups C and D had a significant lower infective viral load in the
278 lungs during the entire post-challenge period (*p<0.01*) and in the brain 4 and 7-8 dpi (*p<0.01*).
279 In the nasal turbinate, a significant lower infective viral load was observed 2 dpi in group D
280 (*p<0.05*) compared with group B, and there was a tendency towards a decrease in group C
281 (*0.05<p<0.1*) 2 dpi and group D (*0.05<p<0.1*) 7-8 dpi compared to group B.
282 Histopathological analyses were performed on lungs and brain of all animals (**Figure 5E**).
283 Infected non-vaccinated animals (group B) had a higher histopathological score in the brain 7-8
284 dpi compared to group C and D (*p<0.01*). No significant differences between groups were
285 observed in the histopathological score of the lungs, but these were numerically higher 4 dpi in
286 group B compared to both vaccinated groups. To support the histopathological scores of
287 **Figure 5E**, we also chose representative sections of brain and lung from study mice showing
288 scores of 0 (lack of lesions), 1 (mild lesions), and 2 (moderate lesions) (**Figure S4**). None of the
289 animals of the study showed lesions with score 3 (severe lesions). Furthermore, other tissues

290 such as spleen, trachea or heart were analysed and no lesions were found in any of the studied
291 animals (**Figure S5 A-C**).

292 **2.4. Recombinant RBD fusion heterodimer antigen immunogenicity and efficacy against**
293 **different SARS-CoV-2 VoCs in K18-hACE2 mice**

294 We next assessed the protective efficacy of PHH-1V vaccine against Beta, Delta and Omicron
295 BA.1 SARS-CoV-2 VoCs in the K18-hACE2 mice model. Animals were vaccinated intramuscularly
296 with two doses of PBS (groups A and B) or 20 µg of PHH-1V vaccine (group C) on D0 and D21,
297 and then animals from groups B and C were intranasally challenged on D35 with Beta, Delta or
298 Omicron BA.1 SARS-CoV-2 variants. Animals were monitored for weight loss and mortality for
299 7 days and then were euthanised at 2, 4 and 7 dpi to analyse viral load in oropharyngeal swabs
300 and lungs by both RT-qPCR and viral titration, and also histopathology in lung sections (**Figure**
301 **6-8**).

302 *2.4.1. Immunogenicity and efficacy of PHH-1V against SARS-CoV-2 Beta variant (B.1.351)*

303 Clinical signs of the SARS-CoV-2 infection were observed only in two animals from the non-
304 vaccinated and infected group (group B) on day 7 post-challenge. Clinical signs curves are
305 shown in **Figure 6A**. Animals from group B had a lower weight ($0.05<p<0.1$) 6 and 7-8 dpi than
306 animals vaccinated with PHH-1V (group C) (**Figure 6B**).

307 SARS-CoV-2 neutralising antibodies against Beta variant were also analysed upon vaccination
308 with PHH-1V in infected K18-hACE2 mice. PHH-1V vaccination elicited higher neutralising titres
309 against Beta variant 0 dpi (D35, pre-challenge) ($p<0.05$) and 7-8 dpi ($p<0.01$) compared to
310 infected control animals (**Figure S2 B**).

311 Viral load was determined in lungs and oropharyngeal swabs by RT-qPCR and $TCID_{50}$ on D37 (2
312 dpi), D39 (4 dpi) and D42 (in males, 7 dpi) or D43 (in females, 8 dpi), or at the time of
313 euthanasia in animals reaching endpoint criteria before the scheduled euthanasia day.
314 Immunisation with 20 µg of PHH-1V (group C) reduced the viral RNA in the lungs 2 dpi
315 ($p<0.01$), 4 dpi ($p<0.05$) and 7-8 dpi ($p<0.01$), but also in oropharyngeal swabs 7-8 dpi ($p<0.01$)

316 compared to the infected control (group B) (**Figure 6C**). Similarly, PHH-1V vaccination reduced
317 the infectious viral load in lungs 2 dpi (*p<0.01*), 4 dpi (*p<0.01*) and 7-8 dpi (*p<0.05*), and also in
318 oropharyngeal swabs 7-8 dpi *(p<0.05)* compared to the infected control (**Figure 6D**).
319 Histopathological scores were also calculated in lung sections from all study animals. Infected
320 control animals had a higher histopathological score in the lung 7-8 dpi compared to PHH-1V
321 vaccinated animals (*p<0.05*).
322 *2.4.2. Immunogenicity and efficacy of PHH-1V against SARS-CoV-1 Delta variant (B.1.617.2)*
323 Clinical signs were observed in all non-vaccinated and infected animals (group B) 6 dpi (2
324 animals) or 7 dpi (4 animals). Three of the six animals showing clinical signs in group B reached
325 the endpoint criteria and were euthanised. In contrast, only one animal of group C showed
326 clinical signs 6 dpi (appearance alteration of score 1). Therefore, curves were significantly
327 different between both groups (B *vs* C; *p<0.05*) (**Figure 7A**). Weight variation was also
328 significantly lower in group B compared to group C from 6 dpi onwards (*p<0.01*) (**Figure 7B**).
329 Neutralising titres induced by PHH-1V vaccine were measured against Delta variant 0 dpi (pre-
330 challenge) and 7-8 dpi (post-challenge). PHH-1V vaccination elicited higher neutralising titres
331 against Delta variant 0 dpi (D35, pre-challenge) and 7-8 dpi (*p<0.01*) compared to infected
332 control animals (group B) (**Figure S2 C**).
333 Viral load was also determined in lungs and oropharyngeal swabs by RT-qPCR and $TCID_{50}$ on
334 D37 (2 dpi), D39 (4 dpi) and D42 (in males, 7 dpi) or D43 (in females, 8 dpi), or at the time of
335 euthanasia in animals reaching endpoint criteria before the scheduled euthanasia day.
336 Immunisation with 20 µg of PHH-1V (group C) reduced the viral RNA in the lungs 2 dpi and 7-8
337 dpi (*p<0.01*), and in oropharyngeal swabs 7-8 dpi (*p<0.05*) compared to the infected control
338 group (**Figure 7C**). Likewise, PHH-1V vaccination reduced the infectious viral load in lungs 2 dpi
339 (*p<0.05*) and 7-8 dpi (*p<0.01*) compared to the infected control group (**Figure 7D**). There was a
340 decreasing trend in the infectious viral load from oropharyngeal swabs of group C 7-8 dpi
341 compared to group B (*0.05<p<0.1*). Furthermore, infected control animals had a higher

342 histopathological score in the lung 7-8 dpi compared to PHH-1V vaccinated animals (*p<0.01*)
343 (**Figure 7E**).

344 *2.4.3. Immunogenicity and efficacy of PHH-1V against SARS-CoV-1 Omicron variant (BA.1)*

345 Additionally, we tested the immunogenicity and efficacy of PHH-1V vaccine against Omicron
346 BA.1, the predominant variant at the time these assays were conducted. No significant
347 differences were observed between groups in clinical signs curves (**Figure 8A**) and weight loss
348 (**Figure 8B**). However, PHH-1V vaccinated animals (group C) showed significantly less viral RNA
349 in lungs 4 dpi (*p<0.05*) (**Figure 8C**) and less infectious SARS-CoV-2 in lungs 4 dpi (*p<0.01*)
350 (**Figure 8D**). There was also a decreasing trend in the viral RNA from oropharyngeal swabs of
351 group C 7-8 dpi compared to group B (*0.05<p<0.1*).

352 Furthermore, neutralising titres induced by PHH-1V vaccine were measured against Omicron
353 BA.1 variant 0 dpi (D35, pre-challenge) and 7-8 dpi (D42-D43, during post-challenge). PHH-1V
354 vaccination elicited higher neutralising titres against Omicron variant 0 dpi and 7-8 dpi (*p<0.01*)
355 compared to infected control animals (group B) (**Figure S2 D**).

356 *2.5. Safety of the recombinant RBD fusion heterodimer antigen after vaccination*

357 The preclinical safety of the PHH-1V candidate vaccine was evaluated in BALB/c mice
358 immunised with different doses of the RBD fusion heterodimer by measuring the bodyweight
359 of each animal once a week until D35/D37. For additional safety information, clinical signs and
360 local reactions were monitored. Differences in bodyweight were observed between the control
361 group and some of the vaccinated groups at different times. The fact that the highest dose
362 (group F) did not show significant differences with the control group during the entire study
363 suggests that these differences in bodyweight are not related to the antigen composition. On
364 the other hand, the differences observed in bodyweight cannot be attributed to the adjuvant
365 because all the PHH-1V vaccines contain the same amount of adjuvant. The mean bodyweight
366 of the control group was above the rest of the groups from the beginning of the study, which
367 could have contributed to the differences observed with the rest of the groups throughout the

368 study (**Figure S1 A**). No clinical signs or local reactions were detected after the vaccinations in
369 BALB/c mice.
370 Additionally, the safety of PHH-1V was evaluated in humanised K18-hACE2 mice, and
371 bodyweight and clinical signs were also monitored during the vaccination period. No
372 significant changes in bodyweight were observed between the different groups (**Figure S1 B**),
373 and vaccinated animals did not show clinical signs or local reactions. The histological
374 evaluation of the injection site revealed a mild lesion (with multifocal mononuclear
375 inflammatory infiltrates within and around muscular fibres) in one of the hind limbs of 1
376 animal vaccinated with the 10-µg RBD fusion heterodimer/dose on D2 and 2 animals
377 vaccinated with the 20-µg RBD fusion heterodimer/dose on D4 post-challenge (**Figure S5 D**).

378 **3. Discussion**

379 In this study, the effect of a recombinant protein RBD fusion heterodimer dose on the
380 immunogenicity and safety of the PHH-1V vaccine was tested in BALB/c and K18-hACE2 mice.
381 Furthermore, the preclinical efficacy of the vaccine candidate was also assessed in SARS-CoV-2-
382 infected and non-infected K18-hACE2 mice, as well as cross-protection induced against Beta,
383 Delta and Omicron BA.1 VoCs. We show that the active substance of the PHH-1V vaccine
384 candidate, the RBD fusion heterodimer, is stable and has an affinity constant of 0.099 nM
385 against the human ACE2 receptor, which indicates an outstanding binding affinity with its
386 natural ligand. The whole sequence of the antigen originates from the SARS-CoV-2 RBD
387 domains of the B.1.1.7 (Alpha) and B.1.351 (Beta) variants, which have been shown by
388 Ramanathan *et al.* to bind ACE2 with increased affinity[34]. We were able to obtain the antigen
389 at high purity, which is consistent with its use as an active drug substance in a vaccine. CHO,
390 the expression system selected to produce this antigen, has been a workhorse to produce
391 monoclonal antibodies and other protein-based therapeutic entities for decades[35]. It has been
392 fully accepted for this purpose by regulatory agencies worldwide.

393 The PHH-1V vaccine candidate was shown to be safe in mice since it did not cause clinical signs
394 (general and local) nor was there any bodyweight loss attributable to the vaccine composition
395 in either immunised BALB/c or K18-hACE2 mice. Although the histological evaluation of the
396 injection sites revealed mild lesions with cellular infiltrates in a few vaccinated animals, these
397 were attributable to the local innate immune response induced upon injection with adjuvant-
398 containing vaccines. Moreover, we have consistently observed an adequate safety profile in
399 other animal species in which the PHH-1V vaccine candidate has been tested, such as rats,
400 rabbits, cynomolgus monkeys and pigs (manuscript in preparation). The SQBA adjuvant used in
401 this vaccine might be related to the good tolerability shown in these animal models.
402 Regarding the RBD-binding antibodies humoral response, a dose response was observed on
403 D35/D37 upon vaccination with RBD heterodimer doses of 0.04, 0.2 and 1 µg/dose. However,
404 this response saturates with higher immunisation doses. Significant total IgG titres were
405 observed after just a single dose for doses of 0.2 µg and above. These results suggest a good
406 potency profile for the antigen included in the PHH-1V vaccine candidate, with similar or
407 superior performance to other previously reported immunogens based on similar
408 platforms[36,37]. Moreover, potent pseudovirus-neutralising activity against the Alpha variant
409 was elicited by the 0.2-µg RBD fusion heterodimer/dose immunisation, reaching the highest
410 titres with the 20-µg RBD fusion heterodimer/dose immunisation. Furthermore, a robust
411 pseudovirus-neutralising activity of sera from mice immunised with 20 µg of RBD fusion
412 heterodimer/dose was confirmed against the Beta, Delta and Omicron BA.1 variants. This
413 cross-reactivity was previously confirmed in earlier exploratory trials, where no significant
414 differences were observed in the pseudovirus-neutralising titres against the Alpha, Beta, and
415 Gamma variants in mice upon vaccination with 20-µg RBD fusion heterodimer/dose. Notably,
416 the pseudovirus neutralisation assays from this work were performed in the same laboratory
417 and under identical conditions as those that were previously reported to have a good
418 correlation with live virus neutralisation assays[38] which highlights the biological relevance of

419 the neutralising antibody titres that were obtained. Even though the recombinant protein RBD
420 fusion heterodimer was designed to elicit a response against the SARS-CoV-2 Alpha and Beta
421 variants, our data also demonstrate a further neutralising activity against the Omicron BA.1
422 variant, the dominant variant around the world at the time when the study was designed[39,40].
423 Indeed, our antigen contains several mutations that are key for being considered of high
424 concern, mutations which are present in currently designated VoCs and which could
425 potentially arise in future variants. That includes the E484K substitution present in the Beta
426 and B.1.621 (mu) variants, as well as the K417N and N501Y mutations present in the Omicron
427 BA.1 variant. E484K is related to immune evasion and reduced antibody neutralisation,
428 compromising the efficacy of the original approved vaccines[41].
429 Regarding cellular response upon vaccination, the ICS data indicate that immunisation with the
430 highest dose of 20-µg RBD fusion heterodimer/dose induced a robust Th1-dominant response
431 with activation of $CD4^+$ and $CD8^+$ T cells expressing IFN-γ and IL-2. Notably, ICS detected no
432 significant IL-4 expression in the splenocytes from immunised animals. However, IL-4 ELISpot
433 assays detected the expression of this Th2 cytokine in splenocytes from both immunised
434 groups. Specifically, according to the ELISpot results, immunisation with the 5-µg RBD fusion
435 heterodimer/dose elicited a Th2-biased response, while immunisation with the 20-µg RBD
436 fusion heterodimer promoted a balanced Th1/Th2 response. These differences in the cytokine
437 expression between both assays might be explained by the differences in the incubation time
438 of the splenocytes after the RBD peptide pool stimulation, which was 48 h for the ELISpot
439 compared to 5 h for the ICS. Furthermore, the experimental conditions (number of splenocytes
440 and incubation time) assayed to detect IFN-γ and IL-4 via ELISpot were different; hence, these
441 data must be interpreted carefully. Th1 immunity is known to be protective for most infections
442 since it promotes humoral immunity as well as phagocytic and cytotoxic T cell activity, whereas
443 the Th2 response assists with the resolution of inflammation[42]. Based on the ICS data,

444 immunisation with the 20-µg RBD fusion heterodimer/dose seems to induce a polarised Th1
445 immune response.
446 Extracellular cytokine production was also measured by Luminex Multiplex in supernatants
447 from splenocytes after 48 h of stimulation, where a balanced production of Th1 (TNF-α, IL-2)
448 and Th2 (IL-5 but no IL-4 nor IL-6) cytokines was found in vaccinated mice. Notably, IFN-γ was
449 not detected by Luminex, probably due to the early expression of this factor and its rapid
450 degradation. Importantly, IL-10 was not detected in the supernatants, which indicates that the
451 immunisation with PHH-1V did not elicit an anti-inflammatory response after the restimulation
452 of splenocytes with RBD peptide pools.
453 The IgG2a/IgG1 ratio was measured to assess Th1/Th2 polarization after the prime-boost
454 immunisation. IgG1 is produced during any type of immune response, while IgG2a is mainly
455 produced during a Th1-polarised immune response[43]. Mice immunised with either the 5-µg or
456 the 20-µg RBD fusion heterodimer/dose induced RBD-binding antibodies of both IgG2a and
457 IgG1 subclasses, with an IgG2a/IgG1 ratio near 0.8, indicating a balanced Th1/Th2 response
458 upon PHH-1V vaccination.
459 Thus, all the data suggest that PHH-1V immunisation with the 20-µg RBD fusion
460 heterodimer/dose elicits a robust $CD4^+$ and $CD8^+$ T cell response with an early expression of
461 Th1 cytokines upon restimulation *in vitro*, and balanced Th1/Th2 cytokine production after 48
462 h post-stimulation.
463 Regarding the preclinical efficacy of the PHH-1V vaccine candidate, it was tested at 2 different
464 doses, 10 µg and 20 µg of RBD fusion heterodimer/dose, in K18-hACE2 mice. Upon the SARS-
465 CoV-2 (Wuhan/D614G strain) challenge, vaccinated animals were able to overcome the
466 infection since neither clinical signs nor bodyweight loss were detected. By contrast, all non-
467 vaccinated and infected animals reached the endpoint criteria on D5 or D6 post-challenge and
468 had to be euthanised. Furthermore, this group of animals experienced remarkable weight loss
469 from D3 post-challenge onwards due to the SARS-CoV-2 infection. Therefore, our data show

470 100% efficacy in preventing mortality and bodyweight loss in infected K18-hACE2 mice upon
471 PHH-1V vaccination.
472 In addition, immunisation with either the 10-µg or the 20-µg RBD fusion heterodimer/dose of
473 PHH-1V reduced the viral load measured via qPCR in the lungs, nasal turbinate, and brain in
474 K18-hACE2 mice. The viral load excretion measured in oropharyngeal swabs was also reduced
475 upon challenge in vaccinated animals. Moreover, differences in the viral load after the SARS-
476 CoV-2 challenge between vaccinated animals and infected non-vaccinated control animals
477 were also found in other respiratory (trachea and pharynx) and systemic (spleen and heart)
478 organs. Notably, when RT-qPCR positive samples were titrated to determine the infective viral
479 load, most of the samples of vaccinated animals showed negative results, whereas most of the
480 samples of the infected control group resulted in significantly higher viral loads. Taken
481 together, these results suggest less viral replication in vaccinated mice, which discards
482 antibody-dependent enhancement (ADE) of the infection upon vaccination. Indeed, RBD is
483 known to pose a low potential for risk of ADE because antibodies against this domain block
484 receptor binding [44]. Likewise, the histopathological evaluation of tissues from vaccinated mice
485 showed no lesions in the brain and mild lesions in the lungs upon SARS-CoV-2 infection. By
486 contrast, infected control mice displayed moderate lesions in the lungs and brain, which is
487 consistent with the high viral loads detected in this group.
488 Notably, preclinical efficacy of PHH-1V vaccine was also assessed in K18-hACE2 mice against
489 Beta, Delta and Omicron BA.1 VoCs. Overall, clinical signs were observed in all non-vaccinated
490 animals infected with the Delta variant, and also in two non-vaccinated animals infected with
491 the Beta variant, while no clinical signs were found in animals vaccinated with 20-µg RBD
492 fusion heterodimer/dose (except 1 mouse). Furthermore, vaccination with 20-µg RBD fusion
493 heterodimer/dose significantly reduced viral load in lungs and oropharyngeal swabs from
494 animals challenged with the Beta and Delta variants. Histopathological scores were also higher
495 in non-vaccinated animals infected with the Beta or Delta variants compared to PHH-1V

496 vaccinated animals. Although there were no significant differences in survival curves and no
497 major clinical signs in the different groups challenged with the Omicron BA.1 variant, viral load
498 was also reduced in lungs from PHH-1V vaccinated animals compared to infected control
499 animals. The reduction of infectivity and pathogenesis of the Omicron BA.1 variant in K18-
500 hACE2 mice has been reported previously in various studies, including a study in which mRNA-
501 1273 protective efficacy was evaluated against Omicron BA.1[45,46]. Hence, PHH-1V vaccination
502 can reduce and control infection of different VoCs, including Omicron BA.1, in lower
503 respiratory airways. This is critical to mitigate the current pandemic situation, although further
504 studies will have to confirm our findings in human subjects.
505 Overall, in this study, the PHH-1V vaccine has been shown to be safe and immunogenic in
506 mice, inducing RBD-binding and neutralising antibodies. Mice immunised with 20 µg of
507 recombinant protein RBD fusion heterodimer/dose showed neutralising activity against the
508 Alpha, Beta, Delta and Omicron BA.1 variants. Likewise, immunisation with 20 µg of RBD fusion
509 heterodimer/dose elicited robust activation of $CD4^+$ and $CD8^+$ T cells, producing an early Th1
510 response upon *in vitro* restimulation. Importantly, vaccination with either the 10-µg or the 20-
511 µg RBD fusion heterodimer/dose prevented weight loss and clinical signs (including mortality)
512 upon SARS-CoV-2 challenge in mice. Both tested doses reduced viral loads in several organs
513 and prevented the infective viral load in the lungs and brain upon experimental infection. In
514 addition, immunisation with 20 µg of RBD recombinant protein fusion heterodimer reduced
515 the infective viral load in the upper respiratory tract (nasal turbinate). Most importantly,
516 vaccination with 20 µg of RBD recombinant protein fusion heterodimer also reduced the
517 infective viral load of Beta, Delta and Omicron BA.1 variants in the lower respiratory tract.
518 Besides the efficacy and safety features of PHH-1V, this second-generation COVID-19 vaccine is
519 easy to adapt to potential emergent SARS-CoV-2 variants, allowing for the inclusion of up to 2
520 different RBDs to generate cross-immunity against emergent variants. The PHH-1V vaccine

521 candidate showed promising preclinical data and is currently being evaluated in Phase I/IIa
522 (NCT05007509), Phase IIb (NCT05142553) and Phase III (NCT05246137) clinical trials[47].

523 **4. Limitations of study:** Although the PHH-1V vaccination reduced the infective viral load of
524 Omicron BA.1 variant in the lower respiratory tract, the K18-hACE2 mice model has shown to
525 be asymptomatic upon the SARS-CoV-2 Omicron BA-1 experimental infection. Therefore other
526 animal model should be addressed to evaluate the prevention of clinical signs after an
527 experimental infection with the SARS-CoV-2 Omicron BA-1 variant.

528 PHH-1V vaccination reduced the infective viral load in the upper respiratory tract after an
529 experimental infection with SARS-CoV-2. However, the local immune response in the upper
530 respiratory tract needs to be analysed in further studies.

531 **5. Acknowledgements**: We would like to thank Marta Ribó, Ariadna Pararols, Rubén
532 Hernández and Helena Sánchez for their assistance in animal care; Jèssica Gómez and Maria
533 Bosch for their support in the tabulation of raw data; Anna Moya, Mireia Muntada, Lidia
534 Galindo and Núria Elias for the ELISA analysis and protein characterisation; Marta Bau for her
535 assistance in the production of the vaccine antigen; Claudia Millán for helping with the
536 modelling and visualisation of the heterodimeric RBD structure; David Solanes Foz for his
537 support to the ABSL3 Unit; the CMCiB Ethical Committee members (Jorge Carrillo, Eulàlia
538 Genescà, Carol Galvez, Carol Soler and Patricia Fachal) for their support in the ethical review of
539 animal procedures; the IGTP Biosafety Committee members (Pere-Joan Cardona, Julià Blanco,
540 Meritxell Carrió, Natalia Ruiz, David Izquierdo and Noemí Parraga) for their support in the
541 review of biosafety procedures; Glòria Pujol and Eduard Fossas for their assistance in the
542 review of the manuscript; Francisco Díaz-Sáez and Anna Muñoz from Alta Medical Services for
543 providing medical writing support; and Adrián Lázaro-Frías from Dynamic Science S.L.U.
544 (Evidenze Clinical Research) for providing medical writing support. We gratefully acknowledge
545 editorial support from Sarah Marshall. This project was partially funded by the Centre for the
546 Development of Industrial Technology (CDTI, IDI20210115), a public organisation answering to

547 the Spanish Ministry of Science and Innovation. Javier Iglesias-Fernández is supported by the
548 Torres Quevedo Programme grant no. PTQ2020-011291 by the Spanish Ministry of Science and
549 Innovation.

550 **6. Author Contributions:** Conceptualisation, Investigation, Methodology, Resources, Formal
551 Analysis and Data Curation: A.B., A.P., L.F., L.M., J.C., A.F., A.Mo., M.C., M.M., G.B., E.P.M.,
552 M.R., R.M., L G., E.P.M., E.P.V., J.P., C.P., T.P.P. & A.M.; Writing Original Draft, Writing – Review
553 & Editing, Visualisation and Supervision: A.B. & A.P.; Investigation: J.R., N.R., M.P., C.L.-O., J.V-
554 A., L.F.-B., J.S., E.P., S.M., B.T., R.O., P.C.R., M.S.-O., J.D., R.A., Y.R. & J.L-C.; Resources: J.I-F, J.V.-
555 A., C.L.-O., J.S., B.T., B.C., J.B., A.M., J.D., Y.R. & S.C.; Writing – Review & Editing: A.Mo, J.V.-A.,
556 C.L.-O., J.S., E.P., B.T., B.C., J.B., A.M., J.D., S.C., J.G-P & J.B.; Supervision: J.V.-A., J.S., B.C., J.B.,
557 A.M., J.G.-P. & J.B.; Project Administration: L.F.; Conceptualisation: T.P.C. & C.G.

558 **7. Competing Interests:** Authors indicated as "1" are employees of HIPRA, a private
559 pharmaceutical company that develops and manufactures vaccines. CReSA, IrsiCaixa, CMCiB-
560 IGTP, UPF and ICREA have received financial support from HIPRA. Two patent applications
561 have been filed by HIPRA SCIENTIFIC S.L.U. and Laboratorios HIPRA, S.A. on different SARS-
562 CoV-2 vaccine candidates and SARS-CoV-2 subunit vaccines, including the recombinant RBD
563 fusion heterodimer PHH-1V. Antonio Barreiro, Antoni Prenafeta, Luis González, Laura Ferrer,
564 Ester Puigvert, Jordi Palmada, Teresa Prat and Carme Garriga are the inventors of these patent
565 applications.

566 **8. Figure Legends**

567 **Figure 1. Structure and characterisation of the B.1.351 (Beta) - B.1.1.7 (Alpha) receptor-**
568 **binding domain (RBD) heterodimer, immunogen of PHH-1V. (A)** Structural representation of
569 the RBD heterodimer. Top: sequence diagram. Bottom left: front view of the RBD heterodimer
570 cartoon structure. Bottom right: top view of the antigen surface structure. Mutations are
571 highlighted in green (K417N), cyan (E484K) and yellow (N501Y). **(B)** Computation modelling for
572 PHH-1V vaccine. Top: AlphaFold2 results for the B.1.351-B.1.1.7 construct. This highlights the

573 presence of two different construct conformations: (i) stabilized N-/C-terminal conformation,
574 and (ii) adopting protein-protein interactions. Bottom: hACE2 receptor-construct model
575 derived from MD calculations of the B.1.351-B.1.1.7 construct. RBD residues 1 to 219 and 220
576 to 439 are shown in grey and orange, respectively, whereas ACE2 monomers are shown as a
577 transparent surface and cartoon representation in violet and purple. **(C)** SDS-PAGE. The
578 reduced and non-reduced purified antigens were loaded at three serial dilutions: 1/10, 1/20
579 and 1/40. M: molecular weight ladder. C: BSA control. **(D)** SEC-HPLC chromatogram of the
580 purified antigen. **(E)** Surface plasmon resonance (SPR) for the quantitative evaluation of the
581 affinity between the antigen and its natural ligand, the human ACE2 receptor. RU: resonance
582 units.

583 **Figure 2. Schematic representation of the experimental protocol in BALB/c and K18-hACE2**
584 **mice for the safety, immunogenicity, and efficacy assessment.** For safety and immunogenicity
585 assays (in the top side), forty-eight 5-week-old female BALB/c mice were allocated to 6 groups
586 (n=8) and were injected intramuscularly with two doses of 0.1 mL of the PHH1-1V vaccine on
587 days 0 (prime) and 21 (boost). Then, animals were monitored daily for clinical signs and
588 bodyweight was recorded weekly until D35/D37, when they were euthanised and both spleens
589 and blood were collected. For safety, immunogenicity and efficacy assays (in the bottom side),
590 K18-hACE2 mice were allocated to 4 groups (efficacy against SARS-CoV-2 D614G) or 3 groups
591 (efficacy against different VoCs), and were injected intramuscularly with two doses of 0.1 mL
592 of the PHH1-1V vaccine on days 0 (prime) and 21 (boost). On D35 animals were challenged
593 with 10^3 $TCID_{50}$ of the SARS-CoV-2 or different VoCs, blood samples were collected to analyse
594 neutralising activity, and they were monitored daily for clinical signs and mortality. Then,
595 challenged animals were chronologically euthanised on D37, D39 and D42/D43; and several
596 tissue samples were collected for several analyses. Schematic artwork used in this figure is
597 provided by Servier Medical Art under a Creative Commons Attribution 3.0 Unported License.

598 **Figure 3. Analysis of the antibody response upon PHH-1V vaccination in mice. (A)** SARS-CoV-2
599 RBD-specific IgG responses in groups A to F on days D0, D21 and D35/D37**.** Endpoint antibody
600 titres determined by ELISA in female BALB/c mice are shown. Log_{10} IgG titres were analysed by
601 means of a linear mixed effects model. **(B)** Endpoint titre ratios of IgG2a to IgG1 in female mice
602 vaccinated with PHH-1V vaccine (groups E and F). Analyses of IgG1 and IgG2 subclasses in
603 groups E and F were performed by ELISA on serum samples taken on day D35/D37. Data was
604 analysed by means of a Mann-Whitney U-test. **(C)** Neutralising antibody responses in groups A
605 to F. SARS-CoV-2 neutralising antibody titres in sera, against pseudoviruses that express the S
606 protein with the Alpha sequence, were determined by PBNA 14/16 days after the second dose
607 of each vaccine (D35/D37). Sera from female BALB/c mice collected on D35/D37 were assessed
608 for pseudovirus-neutralising activity.Log_{10} IC_{50} data was analysed using a generalized least
609 squares (GLS) model, employing one-sample tests against the null H_0: $\mu = 1.78$ for comparison
610 of estimated marginal mean against groups A and B. **(D)** Neutralising antibody responses
611 against multiple SARS-CoV-2 variants (Alpha, Beta, Delta, Omicron BA.1) by PBNA upon 20-µg
612 RBD fusion heterodimer/dose immunization. Sera mice from groups A and F collected on
613 D35/D37 were assessed for pseudovirus-neutralising activity as pool sera or individual sera,
614 respectively. For the analysis of this data, one-sample t-tests against the null H_0: $\mu = 1.78$ were
615 employed. Each data point represents an individual mouse serum, with bars representing the
616 mean titre per group ± SD. Statistically significant differences between groups are indicated
617 with a line on top of each group: * $p<0.05$; ** $p<0.01$; $^{+}$ $0.05<p<0.1$.

618 **Figure 4. PHH-1V-induced $CD4^+$ and $CD8^+$ T cell responses, and extracellular cytokine levels in**
619 **vaccine-induced splenocytes from mice.** Splenocytes from vaccinated female BALB/c mice
620 were isolated 14/16 days after boost immunization (D35/D37), stimulated with RBD peptide
621 pools, and analysed by intracellular cytokine staining. The frequencies of cytokine expressing
622 $CD4^+$ T cells **(A)** and $CD8^+$ T cells **(B)** are shown. The frequencies of $CD4^+$ and $CD8^+$ T cells
623 expressing Th1 cytokines (sum of IFN-γ, TNF-α, IL-2) are also shown. The cytokine expression in

624 splenocytes stimulated with the medium was considered the background value and this was
625 subtracted from peptide-specific responses. Data were analysed using a generalized least
626 squares (GLS) model on the arcsine-square root-transformed percentage values. **(C)**
627 Splenocytes from vaccinated BALB/c mice were isolated 14/16 days after boost immunization
628 (D35/D37), stimulated with RBD peptide pools, and analysed by IFN-γ and IL-4-specific ELISpot
629 assays. Data were analysed using a generalized least squares (GLS) model on the arcsine-
630 square root-transformed percentage values. **(D)** Extracellular cytokines were measured by
631 Luminex Multiplex in supernatants from BALB/c splenocytes stimulated with a pool of peptides
632 from SARS-CoV-2 RBD. Cytokine levels in splenocytes stimulated with the medium were
633 considered the background value and these were subtracted from the responses measured
634 from the RBD peptide pool for each individual mouse. Data were analysed using Kruskal-Wallis'
635 H test and Dunn's post-hoc with Holm's correction for multiple testing or Mann-Whitney's U-
636 test. Each data point represents an individual mouse value, with bars representing the mean ±
637 SD. Statistically significant differences between groups are indicated with a line on top of each
638 group: * $p<0.05$; ** $p<0.01$; $^{+}$ $0.05<p<0.1$.

639 **Figure 5. Protective efficacy of PHH-1V vaccine in K18-hACE2 mice upon SARS-CoV-2**
640 **challenge.** Group A (n=8, 4F + 4M), group B (n=18, 9F + 9M), group C (n=18, 9F + 9M), and
641 group D (n=18, 9F + 9M). **(A)** Survival curves for groups of immunized K18-hACE2 mice with
642 PHH-1V vaccine and control groups. Survival analysis (Kaplan-Meier estimates and log-rank
643 test to compare groups) was performed to study differences in time to/before clinical signs
644 and mortality. **(B)** Mean weight change after SARS-CoV-2 challenge calculated as a percentage
645 of the pre-challenge weight in K18-hACE2 mice. A linear mixed effects model on the body
646 weight change data was performed considering groups B, C and D. Points represent the
647 average weight variation in each group and error bars depict a +/- SD interval. **(C)** SARS-CoV-2
648 RT-qPCR (number of copies) in the lungs, nasal turbinate, oropharyngeal swabs and brain
649 collected from challenged animals. **(D)** Viral titres were determined using a standard

650 $TCID_{50}$ assay on positive samples of RT-qPCR (in some exceptional cases, RT-qPCR and viral
651 isolation were performed in parallel for logistical reasons). RT-qPCR-negative samples are
652 represented as 0 $TCID_{50}$/mL. The detection limit was set at 1.8 $TCID_{50}$/mL. **(E)** Histopathological
653 analyses from the lungs and brain were determined for all animals. For each tissue sample,
654 lesions were classified as follows: multifocal broncho-interstitial pneumonia; multifocal
655 lymphoplasmacytic rhinitis; multifocal lymphoplasmacytic meningoencephalitis; and multifocal
656 mononuclear inflammatory infiltrates within and around muscular fibres. Lesions were
657 evaluated with the following score: 0 (no lesion); 1 (mild lesion); 2 (moderate lesion); and 3
658 (severe lesion). Samples of groups A, C and D correspond to 2 (D37), 4 (D39) and 7 dpi (D42 for
659 males) or 8 dpi (D43 for females); samples of group B were taken 2 (D37), 4 (D39), and 5 dpi
660 (D40; n=3) or 6 dpi (D41; n=3), when animals reached the endpoint criteria. Generalized least
661 squares models or Kruskal-Wallis and Dunn's *post-hoc* tests were employed for the analysis of
662 the RT-qPCR, $TCID_{50}$ and histopathological data depending on verification of assumptions. Each
663 data point represents an individual mouse value, with bars representing the mean ± SD.
664 Statistically significant differences between groups are indicated with a line on top of each
665 group: * $p<0.05$; ** $p<0.01$; $^{+}$ $0.05<p<0.1$. DPI: days post infection. See also **Figures S1-S4.**

666 **Figure 6. Protective efficacy of PHH-1V vaccine in K18-hACE2 mice upon challenge with SARS-**
667 **CoV-2 Beta variant.** Group A (n=8, 4F + 4M), group B (n=18, 9F + 9M), and group C (n=18, 9F +
668 9M). **(A)** Survival curves of animals from PHH-1V vaccinated groups and non-vaccinated
669 groups. Survival analysis (Kaplan-Meier estimates and log-rank test to compare groups) was
670 performed to study differences in time to/before clinical signs and mortality. **(B)** Mean weight
671 change after Beta variant challenge calculated as a percentage of the pre-challenge weight in
672 K18-hACE2 mice. A linear mixed effects model on the body weight change data was performed
673 considering groups B and C. Points represent the average weight variation in each group and
674 error bars depict a +/- SD interval. **(C)** SARS-CoV-2 RT-qPCR (number of copies) in the lungs and
675 oropharyngeal swabs collected from challenged animals. **(D)** Viral titres were determined using

676 a standard $TCID_{50}$ assay on positive samples of RT-qPCR. Negative samples are represented as
677 0 $TCID_{50}$/mL. The detection limit was set at 1.8 $TCID_{50}$/mL. **(E)** Histopathological analyses from
678 the lungs were determined for all animals. For each tissue sample, lesions were classified as
679 follows: multifocal broncho-interstitial pneumonia; multifocal lymphoplasmacytic rhinitis;
680 multifocal lymphoplasmacytic meningoencephalitis; and multifocal mononuclear inflammatory
681 infiltrates within and around muscular fibres. Lesions were evaluated with the following score:
682 0 (no lesion); 1 (mild lesion); 2 (moderate lesion); and 3 (severe lesion). All the samples
683 correspond to 2 (D37), 4 (D39) and 7 dpi (D42 for males) or 8 days post infection (D43 for
684 females); or at the time of euthanasia in animals reaching endpoint criteria before the
685 scheduled euthanasia day. Generalized least squares models or Mann-Whitney tests were
686 employed for the analysis of the RT-qPCR, $TCID_{50}$ and histopathological data depending on
687 verification of assumptions. Each data point represents an individual mouse value, with bars
688 representing the mean ± SD. Statistically significant differences between groups are indicated
689 with a line on top of each group: * $p<0.05$; ** $p<0.01$; $^{+}$ $0.05<p<0.1$. DPI: days post infection.
690 See also **Figure S2.**

691 **Figure 7. Protective efficacy of PHH-1V vaccine in K18-hACE2 mice upon challenge with SARS-**
692 **CoV-2 Delta variant.** Group A (n=8, 4F + 4M), group B (n=18, 9F + 9M), and group C (n=18, 9F +
693 9M), **(A)** Survival curves of animals from PHH-1V vaccinated groups and non-vaccinated
694 groups. Survival analysis (Kaplan-Meier estimates and log-rank test to compare groups) was
695 performed to study differences in time to/before clinical signs and mortality. **(B)** Mean weight
696 change after Delta variant challenge calculated as a percentage of the pre-challenge weight in
697 K18-hACE2 mice. A linear mixed effects model on the body weight change data was performed
698 considering groups B and C. Points represent the average weight variation in each group and
699 error bars depict a +/- SD interval. **(C)** SARS-CoV-2 RT-qPCR (number of copies) in the lungs and
700 oropharyngeal swabs collected from challenged animals. **(D)** Viral titres were determined using
701 a standard $TCID_{50}$ assay on positive samples of RT-qPCR. Negative samples are represented as

702 0 $TCID_{50}$/mL. The detection limit was set at 1.8 $TCID_{50}$/mL. **(E)** Histopathological analyses from
703 the lungs were determined for all animals. For each tissue sample, lesions were classified as
704 previously assays. Lesions were evaluated with the following score: 0 (no lesion); 1 (mild
705 lesion); 2 (moderate lesion); and 3 (severe lesion). All the samples correspond to 2 (D37), 4
706 (D39) and 7 dpi (D42 for males) or 8 days post infection (D43 for females); or at the time of
707 euthanasia in animals reaching endpoint criteria before the scheduled euthanasia day.
708 Generalized least squares models or Mann-Whitney tests were employed for the analysis of
709 the RT-qPCR, $TCID_{50}$ and histopathological data depending on verification of assumptions. Each
710 data point represents an individual mouse value, with bars representing the mean ± SD.
711 Statistically significant differences between groups are indicated with a line on top of each
712 group: * $p<0.05$; ** $p<0.01$; $^{+}$ $0.05<p<0.1$. DPI: days post infection. See also **Figure S2.**

713 **Figure 8. Protective efficacy of PHH-1V vaccine in K18-hACE2 mice upon challenge with SARS-**
714 **CoV-2 Omicron BA.1 variant.** Group A (n=8, 4F + 4M), group B (n=18, 9F + 9M), and group C
715 (n=18, 9F + 9M), **(A)** Survival curves of animals from PHH-1V vaccinated groups and non-
716 vaccinated groups. Survival analysis (Kaplan-Meier estimates and log-rank test to compare
717 groups) was performed to study differences in time to/before clinical signs and mortality. **(B)**
718 Mean weight change after Omicron BA.1 variant challenge calculated as a percentage of the
719 pre-challenge weight in K18-hACE2 mice. A linear mixed effects model on the body weight
720 change data was performed considering groups B and C. Points represent the average weight
721 variation in each group and error bars depict a +/- SD interval. **(C)** SARS-CoV-2 RT-qPCR
722 (number of copies) in the lungs and oropharyngeal swabs collected from challenged animals.
723 **(D)** Viral titres were determined using a standard $TCID_{50}$ assay on positive samples of RT-qPCR.
724 Negative samples are represented as 0 $TCID_{50}$/mL. The detection limit was set at 1.8
725 $TCID_{50}$/mL. **(E)** Histopathological analyses from the lungs were determined for all animals. For
726 each tissue sample, lesions were classified as previously assays. Lesions were evaluated with
727 the following score: 0 (no lesion); 1 (mild lesion); 2 (moderate lesion); and 3 (severe lesion). All

728 the samples correspond to 2 (D37), 4 (D39) and 7 dpi (D42 for males) or 8 days post infection
729 (D43 for females); or at the time of euthanasia in animals reaching endpoint criteria before the
730 scheduled euthanasia day. Generalized least squares models or Mann-Whitney tests were
731 employed for the analysis of the RT-qPCR, $TCID_{50}$ and histopathological data depending on
732 verification of assumptions. Each data point represents an individual mouse value, with bars
733 representing the mean ± SD. Statistically significant differences between groups are indicated
734 with a line on top of each group: * $p<0.05$; ** $p<0.01$; $^{+}$ $0.05<p<0.1$. DPI: days post infection.
735 See also **Figure S2.**

736

737 **9. STAR Methods**

738 **RESOURCE AVAILABILITY**

739 **Lead contact**

740 Requests for further information or data should be directed to and will be fulfilled by the lead
741 contact, Antoni Prenafeta (antoni.prenafeta@hipra.com).

742 **Materials availability**

743 Project-related biological samples are not available since they may be required by regulatory
744 agencies or by HIPRA during the clinical development of the vaccine.

745 **Data and code availability**

746 • Data reported in this study cannot be deposited in a public repository because the
747 vaccine is under clinical evaluation. Upon request, and subject to review, the lead
748 contact will provide the data that support the reported findings.
749 • This paper does not report original code.
750 • Any additional information required to reanalyse the data reported in this paper is
751 available from the lead contact upon request.

752 **EXPERIMENTAL MODEL AND SUBJECT DETAILS**

753 *Animals*

754 BALB/c mice (Envigo, #162) and B6.Cg-Tg(K18-ACE2)2Prlmn/J (K-18-hACE2) transgenic mice
755 (Jackson Laboratories, #034860) were used as animal models. All procedures that involved
756 BALB/c mice were conducted in accordance with the European Union Guidelines for Animal
757 Welfare (Directive 2010/63/EU) and approved by the Ethics Committee of HIPRA Scientific
758 S.L.U. and the Department of Territory and Sustainability of the Catalan Government (file:
759 11388). The experimental procedure that involved the use of K18-hACE2 mice was conducted
760 in accordance with the European Union Guidelines for Animal Welfare (Directive 2010/63/EU)
761 and was approved by the CMCiB Ethics Committee and the Department of Territory and

762 Sustainability of the Catalan Government (file: 11490). The animal study design followed the
763 principles of the 3Rs and animal welfare.
764 Forty-eight 5-week-old female BALB/c mice were allocated to 6 groups (n=8) and were used
765 for safety and immunogenicity assays. BALB/c mice were injected intramuscularly with a 0.1
766 mL/dose of the test vaccine, distributed equally in both hind legs (2 x 50 µL), on days 0 (prime)
767 and 21 (boost). Group A was vaccinated with PBS; group B was immunised with the 0.04-µg
768 recombinant protein RBD fusion heterodimer/dose; group C was immunised with the 0.2-µg
769 recombinant protein RBD fusion heterodimer/dose; group D was immunised with the 1-µg
770 recombinant protein RBD fusion heterodimer/dose; group E was immunised with the 5-µg
771 recombinant protein RBD fusion heterodimer/dose; and group F was immunised with the 20-
772 µg recombinant protein RBD fusion heterodimer/dose. These animals were monitored daily for
773 clinical signs and bodyweight was recorded weekly until D35/D37; at that time, the animals
774 were euthanised and tissues were collected. Animals were watered and fed *ad libitum* with
775 Premium Scientific Diet SAFE® A04 (Safe-lab). Animals were kept on Arbocel® small functional
776 cellulose pellets (Rettenmaier Ibérica, S. L.) with a light/dark cycle of 12 h at a 22 ºC ± 2 ºC in
777 optimum hygienic SPF conditions behind a barrier system under positive pressure with 37 air
778 room renovations per hour. The animals were housed in a stainless-steel rack with
779 polycarbonate cages (530 x 280 x 150 mm) with stainless steel covers equipped with
780 environmental enrichment (nest material: cellulose paper and wood-wool, one PET roll and a
781 PET plastic enrichment dome and a red translucent wheel). The animals were identified with a
782 cage card and individual fur dye. A precision scale (Sartorius, model 112, 6.1 kg with 0.01 g
783 resolution) was used to record the animals' weights.
784 For further safety, immunogenicity, and efficacy assays, sixty-two (31F + 31M) 4/5-week-old
785 K18-humanised ACE2 (hACE2) mice were allocated to 4 groups (n=18; 9F + 9M, except for the
786 placebo group: n=8; 4F + 4M). Specifically, group A was intramuscularly injected with PBS and
787 non-infected; group B was injected with PBS and infected with SARS-CoV-2; group C was

788 vaccinated with 10 µg/dose of recombinant protein RBD fusion heterodimer and infected with
789 SARS-CoV-2; and group D was vaccinated with 20 µg/dose of recombinant protein RBD fusion
790 heterodimer and infected with SARS-CoV-2. Animals from satellite subgroups were euthanised
791 on D35 to assess the immunological response of the vaccinated group. Challenged animals
792 were chronologically euthanised on D37, D39 and D42 (males)/D43 (females). Several tissue
793 samples were collected for further analyses. Efficacy were also assessed against Beta, Delta
794 and Omicron BA.1 variants in three different studies using forty-two 4/5-week-old K18-
795 humanised ACE2 (hACE2) mice. Each study had 2 groups of 18 animal (9F + 9M) and a placebo
796 group of 6 animals (3F + 3M). In particular, group A was intramuscularly injected with PBS and
797 non-infected; group B was injected with PBS and infected with Beta, Delta or Omicron BA.1
798 SARS-CoV-2 variant; and group C was vaccinated with 20 µg/dose of recombinant protein RBD
799 fusion heterodimer and infected with Beta, Delta or Omicron BA.1 SARS-CoV-2 variant.
800 Animals from satellite subgroups were euthanised on D35 to assess the immunological
801 response of the vaccinated group. Challenged animals were also chronologically euthanised on
802 D37, D39 and D42 (males)/D43 (females) in order to collect several tissue samples for RT-qPCR,
803 virus titration and histopathology. Animals were watered and fed *ad libitum* with Teklad Global
804 16% Protein Rodent Diet (Envigo, #2916). Animals were kept on cellulose pellets from
805 Rettenmaier Ibérica. Animals were housed in a ventilated rack, model Blue Line Next/Boxunss
806 (Tecniplast, #1145T00SUV-CP), equipped with environmental enrichment (nest material:
807 cellulose paper and cardboard roll). Animals were kept with a light/dark cycle of 12h at 22 ºC ±
808 2 ºC, with negative room pressure and 20 air renovations per hour. The animals were
809 identified with a dorsal subcutaneous microchip (Trovan, #ID100-B 1.4 Mini transponder). A
810 reader with an integrated scale (Trovan, model 2812005) was used to record the animals'
811 weights. Cibertec was used as the anaesthesia equipment.
812 In order to comply with animal welfare regulations, K18-hACE mice were injected with a 0.1
813 mL/dose of the test vaccine, distributed equally in both hind legs (2 x 50 µL). Vaccines were

814 injected intramuscularly following a two-dose prime-and-boost schedule: 1st dose (prime) on
815 D0 and 2nd dose (boost) on D21. Animals from satellite subgroups were euthanised on D35 to
816 assess the immunological response of the vaccinated group. The SARS-CoV-2 challenge was
817 performed through intranasal inoculation with the strain SARS-CoV-2 Catalonia 02 on a subset
818 of animals on D35 with 25 µL in each nostril (10^3 $TCID_{50}$/mice in 50 µL/mice). This strain
819 (GISAID ID: EPI_ISL_471472), which included the following mutations compared to Wuhan
820 strain, D614G (Spike), K837N (NSP3), P323L (NSP12), was isolated from a male patient from
821 Barcelona, who showed respiratory symptoms. The intranasal experimental infection was
822 performed under sedation with isoflurane 4-5%. The same procedures were followed for
823 infections with SARS-CoV-2 Beta (B.1.351; GISAID EPI_ISL_1663571), Delta (B.1.617.2;
824 GISAID EPI_ISL_3342900) and Omicron (BA.1; GISAID EPI_ISL_8151031) variants.
825 BALB/c mice vaccination and sampling were performed at HIPRA (Girona, Spain). K18-hACE2
826 mice vaccination, SARS-CoV-2 challenge, and sampling were performed in the ABSL3 unit of
827 the Comparative Medicine and Bioimage Centre of Catalonia of the Germans Trias i Pujol
828 Research Institute (Badalona, Spain). The protocol followed is depicted in **Figure 2**.
829 *Cell lines*
830 HEK293T cells overexpressing WT human ACE-2 (Integral Molecular, USA) were used as target
831 in the pseudovirus-based neutralisation assay. Cells were maintained in T75 flasks with
832 Dulbecco's Modified Eagle's Medium (DMEM) supplemented with 10% FBS and 1 µg/mL of
833 Puromycin (Thermo Fisher Scientific, USA).
834 Expi293F cells (Thermo Fisher Scientific) are a HEK293 cell derivative adapted for suspension
835 culture, which were used for SARS-CoV-2 pseudovirus production. Cells were maintained
836 under continuous shaking in Erlenmeyer flasks following the manufacturer's guidelines.
837 Vero E6 (ATCC CRL-1586) cell monolayers were cultured for 3 days at 37 ºC and 5% CO2 in
838 DMEM (GIBCO) supplemented with 100 U/mL penicillin, 100 µg/mL streptomycin and 2 mM
839 glutamine (all reagents from Thermo Fisher Scientific). CHO cells were cultured in a bioreactor

840 in a chemically defined media, at 36-38 ºC with a pH 6.80 - 7.40, 5-8% CO_2 for 60-108 hours
841 with stirring (tip speed 0.4-1) and glucose 2-9 g/L.

842 **METHOD DETAILS**

843 *Computational modelling of antigen constructs*

844 For the estimation of the protein-protein interaction energies of the two studied construct
845 variants (B.1.351-B.1.1.7 and B.1.1.7-B.1.351), AlphaFold2[33] models were generated for each
846 system followed by selection of an individual candidate conformation per construct variant,
847 based on the strongest protein-protein interaction energies identified with the pyDock scoring
848 function[48]. Selected candidates were used as starting models for Molecular Dynamics (MD)
849 simulations with the Amber18 software package[49]. Each protein was immersed in a pre-
850 equilibrated octahedral water box with a 12-Å buffer of TIP3P water molecule[50] using the leap
851 module, resulting in the addition of ~26,000 solvent molecules. The systems were
852 subsequently neutralised by addition of explicit counterions (Na^+ and Cl^-). All calculations were
853 done using the widely tested ff14SB Amber protein force field[51]. A two-stage geometry
854 optimisation approach was performed, consisting of an initial minimisation of solvent
855 molecules and ions (imposing protein restraints of 500 $kcal{\cdot}mol^{-1}{\cdot}Å{-}2$) followed by an
856 unrestrained minimisation of all atoms in the simulation cell. The systems were then gently
857 heated using six 50-ps steps, incrementing the temperature 50 K each step (0–300 K) under
858 constant volume and periodic boundary conditions. Next, both systems were then equilibrated
859 without restraints for 2 ns at a constant pressure of 1 atm and temperature of 300 K. Finally,
860 500 ns MD production simulations were performed for each of the systems in the NVT
861 ensemble and periodic boundary conditions. Models of both constructs bound to a hACE2
862 dimeric receptor were manually built based on available x-ray crystal structures (PDB code:
863 6M17) and MD parameterised following the protocol described above. Production runs of 100
864 ns were calculated for each system studied.

865 The RBD-RBD interaction energies between candidate constructs and construct-hACE2
866 receptor were calculated using the MM-GBSA method in Amber18[52]. For each PHH-1V
867 construct, the MM-GBSA calculation was performed using 300 snapshots over the last 300 ns
868 of the simulation with 1 ns interval with the MMPBSA.py module in Amber 18 with an ionic
869 strength equal to 0.1 M.

870 *Recombinant RBD fusion heterodimer characterisation*

871 The antigen was produced in a bioreactor based on a selected stable CHO clone. A fed-batch
872 strategy was used for high-cell-density cultivation and expression of the RBD fusion
873 heterodimer. Upon harvest, the cell broth was clarified by depth filtration. The clarified
874 supernatant was further purified via sequential chromatography. The purified antigen was
875 then buffer exchanged by tangential flow filtration and filter sterilised. Purity and integrity
876 were evaluated by SDS-PAGE with Bolt™ 4 to 12% Bis-Tris gels (Thermo Fisher, ref.
877 NW04120BOX), stained with One-Step Blue Protein Gel Stain (Biotium, ref. 21003), and by SEC-
878 HPLC with an Xbridge Protein BEH SEC (Waters, ref. 186009160) connected to an HP1100
879 system (Agilent Technologies).

880 The affinity test of the RBD heterodimer with human ACE2 by surface plasmon resonance (SPR)
881 was performed by ACROBiosystems. The Fc-tagged ACE2 (AC2-H5257, ACROBiosystems) was
882 immobilised in a Series S Sensor Chip CM5 (Cytiva) on a Biacore T200 (Cytiva) using the Human
883 Antibody Capture Kit (Cytiva). The affinity measure was obtained using 8 different RBD
884 heterodimer concentrations. The antigen structure simulations were performed with UCSF
885 ChimeraX[53].

886 *SARS-CoV-2 recombinant protein RBD heterodimer adjuvanted vaccines*

887 The purified RBD fusion heterodimer was formulated with the SQBA adjuvant, an oil-in-water
888 emulsion produced by HIPRA. The PHH-1V vaccine was tested at different concentrations: 0.04
889 µg, 0.2 µg, 1 µg, 5 µg and 20 µg of RBD fusion heterodimer/dose for the safety and
890 immunogenicity assays in BALB/c mice. For efficacy assessment in the K18-hACE2 mice animal

891 model, the vaccine was tested at 10 µg and 20 µg of fusion heterodimer/dose. The placebo
892 vaccines were prepared with phosphate-buffered saline (PBS).

893 *Analysis of SARS-CoV-2-specific antibodies*

894 Serum binding antibodies against SARS-CoV-2 RBD were determined by ELISA (HIPRA).
895 MaxiSorp plates (Nunc, Roskilde, Denmark) were coated with 100 ng/well RBD protein (Sino
896 Biologicals, Beijing, China) and blocked with 5% non-fat dry milk (Difco™ Skim Milk, BD,
897 Franklin Lakes, NJ, USA) in PBS. Wells were incubated with serial dilutions of the serum
898 samples and the bound total IgG specific antibodies were detected by peroxidase-conjugated
899 Goat Anti-Mouse IgG (Sigma-Aldrich, St. Louis, MO, USA). Finally, wells were incubated with K-
900 Blue Advanced Substrate (Neogen, Lansing, MI, USA) and the absorbance at 450 nm was
901 measured using a microplate reader (Versamax microplate reader, Molecular Devices, San
902 Jose, CA, USA). The mean value of the absorbance was calculated for each dilution of the
903 serum sample run in duplicate. Isotypes IgG1 and IgG2a were detected using Peroxidase
904 AffiniPure Goat Anti-Mouse IgG, Fcγ subclass 1 specific, and Peroxidase AffiniPure Goat Anti-
905 Mouse IgG, Fcγ subclass 2a specific, (Jackson ImmunoResearch, Cambridge, UK), respectively.
906 The endpoint titre of RBD-specific total IgG binding antibodies was established as the
907 reciprocal of the last serum dilution yielding 3 times the mean optical density of the negative
908 control of the technique (wells without serum added).

909 *Pseudovirus neutralisation assay*

910 Neutralising antibodies in serum against SARS-CoV-2 Wuhan (original sequence) and the Alpha,
911 Beta, Gamma, and Delta variants were determined by a pseudoviruses-based neutralisation
912 assay (PBNA) at IRSICaixa (Barcelona, Spain) using an HIV reporter pseudovirus that expresses
913 the S protein of SARS-CoV-2 and luciferase. To generate pseudoviruses, Expi293F cells were
914 transfected using ExpiFectamine293 Reagent (Thermo Fisher Scientific) with pNL4-3.Luc.R-.E-
915 and SARS-CoV-2.SctΔ19 at a 24:1 ratio, respectively[54]. pNL4-3.Luc.R-.E- was obtained from the
916 NIH AIDS Reagent Program and SARS-CoV-2.SctΔ19 was generated by GeneArt from the full

917 protein sequence of SARS-CoV-2 spike with a deletion of the last 19 amino acids in C-
918 terminal,24 human-codon optimized and inserted into pcDNA3.4-TOPO. Control pseudoviruses
919 were obtained by replacing the S protein expression plasmid with a VSV-G protein expression
920 plasmid (pVSV-G) described before[55]. Supernatants were harvested 48 hours after
921 transfection, filtered at 0.45 mm, frozen, and titrated on HEK293T cells overexpressing WT
922 human ACE-2 (Integral Molecular, USA).
923 For the neutralisation assay, 200 $TCID_{50}$ of pseudovirus supernatant was preincubated with
924 serial dilutions of the heat-inactivated serum samples for 1 h at 37 °C and then added onto
925 ACE2 overexpressing HEK293T cells. After 48 h, cells were lysed with britelite plus luciferase
926 reagent (PerkinElmer, Waltham, MA, USA). Luminescence was measured for 0.2 s with an
927 EnSight multimode plate reader (PerkinElmer). The neutralisation capacity of the serum
928 samples was calculated by comparing the experimental RLU calculated from infected cells
929 treated with each serum to the max RLUs (maximal infectivity calculated from untreated
930 infected cells) and min RLUs (minimal infectivity calculated from uninfected cells) and
931 expressed as the neutralisation percentage: neutralisation[38] (%) = (RLUmax–
932 RLUexperimental)/(RLUmax–RLUmin) * 100. IC_{50} were calculated by plotting and fitting
933 neutralisation values and the plasma dilution log to a 4-parameters equation in Prism 9.0.2
934 (GraphPad Software, USA).
935 *Intracellular cytokine staining (ICS)*
936 ICS was performed by the Infection Biology Group at the Department of Experimental and
937 Health Sciences, Universitat Pompeu Fabra (DCEXS-UPF, Barcelona, Spain). Spleens from
938 female mice were mechanically disrupted onto a 40-µM cell strainer and incubated in 5 mL of
939 0.15 M ammonium chloride buffer for 5 min at room temperature (RT) for red blood cell lysis.
940 Cells were then washed in RPMI (Gibco, Tavarnuzze, Italy) supplemented with 10% FBS, 1%
941 penicillin/streptomycin, 0.05 mM-Mercaptoethanol and 1 mM sodium pyruvate (cRPMI). Two
942 million splenocytes per well (96-well plate) were stimulated in vitro under three conditions: (i)

943 a 1:1 mix of the peptide libraries (PepMix™) from the B.1.1.7 (Alpha variant) and B.1.351 (Beta
944 variant) lineages covering the entire RBD of the SARS-CoV-2 S protein; (ii) cRPMI (negative
945 control); and (iii) PMA + Ionomycin (positive control) for 5 h at 37 ºC 5% CO_2 in cRPMI in the
946 presence of Brefeldin A (Sigma-Aldrich) for the last 3 h before antibody staining. The final
947 concentrations used were 1 µg/mL of each peptide of the RBD peptide pool, 15 ng/mL of PMA
948 (Sigma-Aldrich) and 250 ng/mL of ionomycin (Sigma-Aldrich). For flow cytometric analysis,
949 equal numbers of cells were stained with Fixable Viability Stain 780 (BD Biosciences, New
950 Jersey, NJ, USA) in PBS for 15 min at RT followed by staining with antibodies against CD3, CD4,
951 CD8 and CD44 for 20 min on ice in FACS buffer (PBS: 5% FCS, 0.5% BSA, 0.07% NaN3). Cells
952 were then fixed for 20 min on ice with 2% formaldehyde and stained with antibodies against
953 intracellular proteins (IFN-γ, TNF-α, IL-2 and IL-4) for 20 min on ice in perm/wash buffer (PBS:
954 1% FCS, NaN3 0.1%, saponin 0.1%). All antibodies were purchased from either BD Biosciences,
955 Thermo Fisher or BioLegend (see Table S1 for more details). Samples were processed on an
956 Aurora analyser (Cytek, Fremont, CA, USA). FACS data were analysed using FlowJo 10 software
957 (Tree Star Inc., Ashland, OR, USA). The gating strategy followed in the analysis is depicted in
958 **Figure S6**. The stain index was calculated by subtracting the mean fluorescence intensity (MFI)
959 of the unstained or fluorescence minus one (FMO) control from the MFI of the stained samples
960 and dividing it by two times the standard deviation of the unstained population. Background
961 cytokine expression in the no-peptide (cRPMI) condition was subtracted from that measured in
962 the RBD peptide pool for each mouse. To calculate the Th1 response in $CD4^+$ and $CD8^+$, the
963 Boolean tool of the FlowJo software was used.

964 *Mouse cytokine assay*

965 The cytokine assay was performed by the Infection Biology Group at the Department of
966 Experimental and Health Sciences, Universitat Pompeu Fabra (DCEXS-UPF, Barcelona, Spain).
967 Splenocytes from female mice were seeded at 1.1×10^6 cells/well in 24-well plates and
968 stimulated with a 1:1 mix of the RBD overlapping peptides from B.1.1.7 (Alpha variant) and

969 B.1.1351 (Beta variant) lineages (1 µg/mL each). cRPMI media was used as a negative control
970 and PMA (15 ng/mL) + ionomycin (250 ng/mL) as a positive control. The supernatants were
971 harvested after 48 h incubation at 37 °C and a panel that quantifies the cytokines IL-2, IL-4, IL-
972 5, IL-6, IL-10, IFN-γ and TNF-α (Luminex Multiplex, Invitrogen, Waltham, MA, USA) was run
973 according to the manufacturer's instructions. These measurements were performed at
974 Veterinary Clinical Biochemistry Service, Faculty of Veterinary Medicine, Universitat Autònoma
975 de Barcelona (UAB, Barcelona, Spain).

976 *IFN-γ and IL-4 ELISpot assays*

977 ELISpot assays were performed with mouse IFN-γ and IL-4 ELISpot PLUS kits according to the
978 manufacturer's instructions (3321-4HPT-10 and 3311-4HPW-10, Mabtech, Herndon, VA, USA).
979 A total of 2.5×10^5 or 4×10^5 splenocytes from female mice were seeded per well for the IFN-γ
980 and IL-4 tests, respectively, and *ex vivo* stimulated either with the 1:1 mix of the RBD
981 overlapping peptides from the B.1.1.7 (Alpha variant) and B.1.351 (Beta variant) lineages (1
982 µg/mL each), or with complete cRPMI (negative control) or with concanavalin A (5 µg/mL
983 (Sigma-Aldrich)) (positive control). Each condition was run in duplicates. After an incubation
984 period of 18-20 h (for IFN-γ) or 48 h (for IL-4), the plates were manipulated according to the
985 manufacturer's instructions. Spots were counted under a dissection microscope. Frequencies
986 of IFN-γ or IL-4-secreting cells were expressed as the number of responding cells per million
987 splenocytes. The number of spots in unstimulated cultures (negative control) was subtracted
988 from the spot count in RBD-stimulated cultures.

989 *SARS-CoV-2 genomic RT-qPCR*

990 Total viral load in respiratory tissue samples was determined by RT-qPCR (CReSA, IRTA-UAB,
991 Barcelona, Spain). Viral RNA was extracted from target organs and swabs samples using the
992 IndiMag pathogen kit (Indical Bioscience) on a Biosprint 96 workstation (QIAGEN) according to
993 the manufacturer's instructions. The RT-qPCR used to detect viral gRNA was performed with
994 the AgPath-ID One-Step RT-PCR Kit (Life Technologies). In brief, 5 µL of RNA were added to 25

995 µL reaction containing 12.5 µL of 2 × reaction buffer and 1 µL of 25X RT-PCR Enzyme mix
996 provided with ArrayScript™ Reverse Transcriptase and AmpliTaq Gold® DNA Polymerase. RT-
997 qPCR targets a portion of the envelope protein gene (position 26,141–26,253 of GenBank
998 NC_004718). The primers and probes used, and their final concentration, were the following:
999 forward, 5′-ACAGGTACGTTAATAGTTAATAGCGT-3′ [400 nM]; reverse, 5′-
1000 ATATTGCAGCAGTACGCACACA-3′ [400 nM]; probe, 5′-FAM-ACACTAGCCATCCTTA
1001 CTGCGCTTCG-TAMRA-3′ [200 nM][56]. Thermal cycling was performed at 55 °C for 10 min for
1002 reverse transcription, followed by 95 °C for 3 min, and then 45 cycles of 94 °C for 15 s plus 58
1003 °C for 30 s.

1004 *Virus titration in Vero E6 cell*

1005 Virus titres were determined in RT-qPCR positive samples using a standard $TCID_{50}$ assay in Vero
1006 E6 cells at CReSA (IRTA-UAB) [56]. Briefly, each sample was 10-fold diluted in duplicate,
1007 transferred in a 96 well plate with a Vero E6 cells monolayer and incubated at 37 °C and 5%
1008 CO_2. Plates were monitored daily under the light microscope and wells were evaluated for the
1009 presence of CPE at 5 dpi. The amount of infectious virus was calculated by determining the
1010 $TCID_{50}$ using the Reed-Muench method.

1011 *Histopathology*

1012 Histopathological analyses were performed at CReSA (IRTA-UAB). Lower (lungs) respiratory
1013 tract, brain, spleen, trachea, heart and skeletal muscle were fixed in 10% buffered formalin
1014 and routinely processed for histopathology. Haematoxylin- and eosin-stained slides were
1015 examined under optical microscope. Multifocal broncho-interstitial pneumonia, multifocal
1016 lymphoplasmacytic rhinitis and non-suppurative meningoencephalitis were evaluated from
1017 lung, nasal turbinate and brain lesions, respectively, according to the following semi-
1018 quantitative score: 0 (no lesion); 1 (mild lesion, multifocal distribution and less than 10% of
1019 tissue affected); 2 (moderate lesion, multifocal distribution and between 10-40% of tissue
1020 affected); and 3 (severe lesion, multifocal to diffuse distribution and more than 40% of tissue

1021 affected)[56,57]. A European certified (ECVP) pathologist performed a blinded pathology
1022 assessment.

1023 **QUANTIFICATION AND STATISTICAL ANALYSIS**

1024 Statistical analyses and plots were generated using R (version 4.0.5) or GraphPad Prism
1025 (version 9). Unless otherwise specified, all plots depict individual data points for each animal,
1026 along with the sample mean and standard deviation. When required, data was either $\log_{10}$- or
1027 arcsine-transformed (i.e., log-normal and percentage variables, respectively). The exact
1028 number (n) used in each experiment is indicated in the caption below each figure.

1029 When testing the effect of one or two factors, one-way ANOVA or linear models were
1030 generally employed. For models involving independent observations, the generalised least
1031 squares approximation (GLS implementation in the R package nlme) was used to
1032 accommodate potential heteroscedasticity. Conversely, for models involving repeated
1033 measures, linear mixed effects models were fitted using the lme implementation in the R
1034 package nlme. Unless otherwise specified, time, group and their interaction were included in
1035 the models as fixed effects, and the experimental subject was considered a random factor. The
1036 corresponding random intercept models were fitted to the data using restricted maximum
1037 likelihood. Correlation between longitudinal observations as well as heteroscedasticity were
1038 included in the models when required with appropriate variance-covariance structures. On the
1039 other hand, data violating the assumption of normality, as well as ordinal variables, were
1040 analysed using Mann-Whitney or Kruskal-Wallis tests, depending on the number of groups,
1041 segregating by timepoint if needed.

1042 Assumptions were tested graphically (using quantile-quantile and residual plots) for both
1043 modelling approaches, and model selection was based on likelihood ratio tests or a priori
1044 assumptions. The corresponding estimated marginal means were calculated using the R
1045 package emmeans.

1046 For post-hoc pairwise comparisons, appropriate tests were employed depending on the nature
1047 of the data and the comparisons to perform, with corrections for multiple testing when
1048 required (i.e., Holm's-Bonferroni correction or multivariate t-distribution adjustment). When
1049 comparisons against zero-variance groups (all observations having the same value) needed to
1050 be performed, one-sample tests were employed instead.
1051 Finally, survival analysis was performed to test the differences in clinical signs and mortality
1052 using Kaplan-Meier estimates and the log-rank test. For analyses involving more than two
1053 groups, a priori pairwise contrasts were employed upon significant omnibus log-rank tests to
1054 control type I error.
1055 Statistically significant differences between groups are indicated with a line on top of each
1056 group: ** $p<0.01$; * $p<0.05$; $^{+}$ $0.05<p<0.1$.
1057 **KEY RESOURCES TABLE:** See attached document.
1058 **10. Supplemental Information:** See attached document.
1059

1060 **11. References**

1061 1. WHO (2021). WHO Coronavirus (COVID-19) Dashboard. https://covid19.who.int/.
1062 2. Mathieu, E., Ritchie, H., Ortiz-Ospina, E., Roser, M., Hasell, J., Appel, C., Giattino, C., and
1063 Rodés-Guirao, L. (2021). Author Correction: A global database of COVID-19 vaccinations.
1064 Nat Hum Behav *5*, 956-959. 10.1038/s41562-021-01160-2.
1065 3. Ritchie, H., Rodés-Guirao, L., Appel, C., Giattino, C., Ortiz-Ospina, E., Hasell, J., Macdonald,
1066 B., Beltekian, D., and Roser, M. (2022). Coronavirus Pandemic (COVID-19).
1067 https://ourworldindata.org/coronavirus.
1068 4. Günl, F., Mecate-Zambrano, A., Rehländer, S., Hinse, S., Ludwig, S., and Brunotte, L. (2021).
1069 Shooting at a Moving Target-Effectiveness and Emerging Challenges for SARS-CoV-2 Vaccine
1070 Development. Vaccines (Basel) *9*. 10.3390/vaccines9101052.
1071 5. Moyo-Gwete, T., Madzivhandila, M., Makhado, Z., Ayres, F., Mhlanga, D., Oosthuysen, B.,
1072 Lambson, B.E., Kgagudi, P., Tegally, H., Iranzadeh, A., et al. (2021). SARS-CoV-2 501Y.V2
1073 (B.1.351) elicits cross-reactive neutralizing antibodies. bioRxiv. 10.1101/2021.03.06.434193.
1074 6. Mellet, J., and Pepper, M.S. (2021). A COVID-19 Vaccine: Big Strides Come with Big
1075 Challenges. Vaccines (Basel) *9*. 10.3390/vaccines9010039.
1076 7. Alanagreh, L., Alzoughool, F., and Atoum, M. (2020). The Human Coronavirus Disease
1077 COVID-19: Its Origin, Characteristics, and Insights into Potential Drugs and Its Mechanisms.
1078 Pathogens *9*. 10.3390/pathogens9050331.
1079 8. Vogel, A.B., Kanevsky, I., Che, Y., Swanson, K.A., Muik, A., Vormehr, M., Kranz, L.M., Walzer,
1080 K.C., Hein, S., Güler, A., et al. (2020). A prefusion SARS-CoV-2 spike RNA vaccine is highly
1081 immunogenic and prevents lung infection in non-human primates. bioRxiv,
1082 2020.2009.2008.280818. 10.1101/2020.09.08.280818.
1083 9. Zhou, P., Yang, X.L., Wang, X.G., Hu, B., Zhang, L., Zhang, W., Si, H.R., Zhu, Y., Li, B., Huang,
1084 C.L., et al. (2020). Addendum: A pneumonia outbreak associated with a new coronavirus of
1085 probable bat origin. Nature *588*, E6. 10.1038/s41586-020-2951-z.
1086 10. Huang, Y., Yang, C., Xu, X.F., Xu, W., and Liu, S.W. (2020). Structural and functional
1087 properties of SARS-CoV-2 spike protein: potential antivirus drug development for COVID-19.
1088 Acta Pharmacol Sin *41*, 1141-1149. 10.1038/s41401-020-0485-4.
1089 11. Yi, C., Sun, X., Ye, J., Ding, L., Liu, M., Yang, Z., Lu, X., Zhang, Y., Ma, L., Gu, W., et al. (2020).
1090 Key residues of the receptor binding motif in the spike protein of SARS-CoV-2 that interact
1091 with ACE2 and neutralizing antibodies. Cell Mol Immunol *17*, 621-630. 10.1038/s41423-
1092 020-0458-z.
1093 12. Cao, Y., Wang, J., Jian, F., Xiao, T., Song, W., Yisimayi, A., Huang, W., Li, Q., Wang, P., An, R.,
1094 et al. (2022). Omicron escapes the majority of existing SARS-CoV-2 neutralizing antibodies.
1095 Nature *602*, 657-663. 10.1038/s41586-021-04385-3.
1096 13. Liu, Z., Xu, W., Xia, S., Gu, C., Wang, X., Wang, Q., Zhou, J., Wu, Y., Cai, X., Qu, D., et al.
1097 (2020). RBD-Fc-based COVID-19 vaccine candidate induces highly potent SARS-CoV-2
1098 neutralizing antibody response. Signal Transduct Target Ther *5*, 282. 10.1038/s41392-020-
1099 00402-5.
1100 14. Plante, J.A., Mitchell, B.M., Plante, K.S., Debbink, K., Weaver, S.C., and Menachery, V.D.
1101 (2021). The variant gambit: COVID-19's next move. Cell Host Microbe *29*, 508-515.
1102 10.1016/j.chom.2021.02.020.
1103 15. WHO (2022). Tracking SARS-CoV-2 variants. https://www.who.int/activities/tracking-SARS-
1104 CoV-2-variants.

1105 16. Dai, L., and Gao, G.F. (2021). Viral targets for vaccines against COVID-19. Nat Rev Immunol
1106 *21*, 73-82. 10.1038/s41577-020-00480-0.
1107 17. Pallesen, J., Wang, N., Corbett, K.S., Wrapp, D., Kirchdoerfer, R.N., Turner, H.L., Cottrell,
1108 C.A., Becker, M.M., Wang, L., Shi, W., et al. (2017). Immunogenicity and structures of a
1109 rationally designed prefusion MERS-CoV spike antigen. Proc Natl Acad Sci U S A *114*, E7348-
1110 e7357. 10.1073/pnas.1707304114.
1111 18. EMA (2021). Comirnaty : EPAR - Product information.
1112 https://www.ema.europa.eu/en/documents/product-information/comirnaty-epar-product-
1113 information_en-0.pdf.
1114 19. EMA (2021). Spikevax (previously COVID-19 Vaccine Moderna): EPAR - Product information.
1115 https://www.ema.europa.eu/en/documents/product-information/spikevax-previously-
1116 covid-19-vaccine-moderna-epar-product-information_en.pdf.
1117 20. EMA (2022). Jcovden (previously COVID-19 Vaccine Janssen).
1118 https://www.ema.europa.eu/en/medicines/human/EPAR/jcovden-previously-covid-19-
1119 vaccine-janssen.
1120 21. Keech, C., Albert, G., Cho, I., Robertson, A., Reed, P., Neal, S., Plested, J.S., Zhu, M., Cloney-
1121 Clark, S., Zhou, H., et al. (2020). Phase 1-2 Trial of a SARS-CoV-2 Recombinant Spike Protein
1122 Nanoparticle Vaccine. N Engl J Med *383*, 2320-2332. 10.1056/NEJMoa2026920.
1123 22. Francica, J.R., Flynn, B.J., Foulds, K.E., Noe, A.T., Werner, A.P., Moore, I.N., Gagne, M.,
1124 Johnston, T.S., Tucker, C., Davis, R.L., et al. (2021). Vaccination with SARS-CoV-2 Spike
1125 Protein and AS03 Adjuvant Induces Rapid Anamnestic Antibodies in the Lung and Protects
1126 Against Virus Challenge in Nonhuman Primates. bioRxiv. 10.1101/2021.03.02.433390.
1127 23. Goepfert, P.A., Fu, B., Chabanon, A.L., Bonaparte, M.I., Davis, M.G., Essink, B.J., Frank, I.,
1128 Haney, O., Janosczyk, H., Keefer, M.C., et al. (2021). Safety and immunogenicity of SARS-
1129 CoV-2 recombinant protein vaccine formulations in healthy adults: interim results of a
1130 randomised, placebo-controlled, phase 1-2, dose-ranging study. Lancet Infect Dis *21*, 1257-
1131 1270. 10.1016/s1473-3099(21)00147-x.
1132 24. Kyriakidis, N.C., López-Cortés, A., González, E.V., Grimaldos, A.B., and Prado, E.O. (2021).
1133 SARS-CoV-2 vaccines strategies: a comprehensive review of phase 3 candidates. NPJ
1134 Vaccines *6*, 28. 10.1038/s41541-021-00292-w.
1135 25. Kleanthous, H., Silverman, J.M., Makar, K.W., Yoon, I.K., Jackson, N., and Vaughn, D.W.
1136 (2021). Scientific rationale for developing potent RBD-based vaccines targeting COVID-19.
1137 NPJ Vaccines *6*, 128. 10.1038/s41541-021-00393-6.
1138 26. Gavi Alliance, C.c.p. (2020). What are protein subunit vaccines and how could they be used
1139 against COVID-19? https://www.gavi.org/vaccineswork.
1140 27. Piccoli, L., Park, Y.J., Tortorici, M.A., Czudnochowski, N., Walls, A.C., Beltramello, M., Silacci-
1141 Fregni, C., Pinto, D., Rosen, L.E., Bowen, J.E., et al. (2020). Mapping Neutralizing and
1142 Immunodominant Sites on the SARS-CoV-2 Spike Receptor-Binding Domain by Structure-
1143 Guided High-Resolution Serology. Cell *183*, 1024-1042.e1021. 10.1016/j.cell.2020.09.037.
1144 28. Wang, H., Wu, X., Zhang, X., Hou, X., Liang, T., Wang, D., Teng, F., Dai, J., Duan, H., Guo, S.,
1145 et al. (2020). SARS-CoV-2 Proteome Microarray for Mapping COVID-19 Antibody
1146 Interactions at Amino Acid Resolution. ACS Cent Sci *6*, 2238-2249.
1147 10.1021/acscentsci.0c00742.
1148 29. Greaney, A.J., Loes, A.N., Crawford, K.H.D., Starr, T.N., Malone, K.D., Chu, H.Y., and Bloom,
1149 J.D. (2021). Comprehensive mapping of mutations in the SARS-CoV-2 receptor-binding

1150 domain that affect recognition by polyclonal human plasma antibodies. Cell Host Microbe
1151 *29*, 463-476.e466. 10.1016/j.chom.2021.02.003.
1152 30. Greaney, A.J., Loes, A.N., Gentles, L.E., Crawford, K.H.D., Starr, T.N., Malone, K.D., Chu, H.Y.,
1153 and Bloom, J.D. (2021). Antibodies elicited by mRNA-1273 vaccination bind more broadly to
1154 the receptor binding domain than do those from SARS-CoV-2 infection. Sci Transl Med *13*.
1155 10.1126/scitranslmed.abi9915.
1156 31. Lee, W.S., Wheatley, A.K., Kent, S.J., and DeKosky, B.J. (2020). Antibody-dependent
1157 enhancement and SARS-CoV-2 vaccines and therapies. Nat Microbiol *5*, 1185-1191.
1158 10.1038/s41564-020-00789-5.
1159 32. Cox, J.C., and Coulter, A.R. (1997). Adjuvants--a classification and review of their modes of
1160 action. Vaccine *15*, 248-256. 10.1016/s0264-410x(96)00183-1.
1161 33. Jumper, J., Evans, R., Pritzel, A., Green, T., Figurnov, M., Ronneberger, O., Tunyasuvunakool,
1162 K., Bates, R., Žídek, A., Potapenko, A., et al. (2021). Highly accurate protein structure
1163 prediction with AlphaFold. Nature *596*, 583-589. 10.1038/s41586-021-03819-2.
1164 34. Ramanathan, M., Ferguson, I.D., Miao, W., and Khavari, P.A. (2021). SARS-CoV-2 B.1.1.7 and
1165 B.1.351 Spike variants bind human ACE2 with increased affinity. bioRxiv.
1166 10.1101/2021.02.22.432359.
1167 35. Sharker, S.M., and Rahman, A. (2021). A Review on the Current Methods of Chinese
1168 Hamster Ovary (CHO) Cells Cultivation for the Production of Therapeutic Protein. Curr Drug
1169 Discov Technol *18*, 354-364. 10.2174/1570163817666200312102137.
1170 36. Kuo, T.Y., Lin, M.Y., Coffman, R.L., Campbell, J.D., Traquina, P., Lin, Y.J., Liu, L.T., Cheng, J.,
1171 Wu, Y.C., Wu, C.C., et al. (2020). Development of CpG-adjuvanted stable prefusion SARS-
1172 CoV-2 spike antigen as a subunit vaccine against COVID-19. Sci Rep *10*, 20085.
1173 10.1038/s41598-020-77077-z.
1174 37. Tian, J.H., Patel, N., Haupt, R., Zhou, H., Weston, S., Hammond, H., Logue, J., Portnoff, A.D.,
1175 Norton, J., Guebre-Xabier, M., et al. (2021). SARS-CoV-2 spike glycoprotein vaccine
1176 candidate NVX-CoV2373 immunogenicity in baboons and protection in mice. Nat Commun
1177 *12*, 372. 10.1038/s41467-020-20653-8.
1178 38. Trinité, B., Tarrés-Freixas, F., Rodon, J., Pradenas, E., Urrea, V., Marfil, S., Rodríguez de la
1179 Concepción, M.L., Ávila-Nieto, C., Aguilar-Gurrieri, C., Barajas, A., et al. (2021). SARS-CoV-2
1180 infection elicits a rapid neutralizing antibody response that correlates with disease severity.
1181 Sci Rep *11*, 2608. 10.1038/s41598-021-81862-9.
1182 39. Hadfield, J., Megill, C., Bell, S.M., Huddleston, J., Potter, B., Callender, C., Sagulenko, P.,
1183 Bedford, T., and Neher, R.A. (2018). Nextstrain: real-time tracking of pathogen evolution.
1184 Bioinformatics *34*, 4121-4123. 10.1093/bioinformatics/bty407.
1185 40. Nextstrain (2021). Genomic epidemiology of novel coronavirus - Global subsampling.
1186 https://nextstrain.org/ncov/gisaid/global/6m.
1187 41. Jangra, S., Ye, C., Rathnasinghe, R., Stadlbauer, D., Krammer, F., Simon, V., Martinez-
1188 Sobrido, L., García-Sastre, A., and Schotsaert, M. (2021). SARS-CoV-2 spike E484K mutation
1189 reduces antibody neutralisation. Lancet Microbe *2*, e283-e284. 10.1016/s2666-
1190 5247(21)00068-9.
1191 42. Spellberg, B., and Edwards, J.E., Jr. (2001). Type 1/Type 2 immunity in infectious diseases.
1192 Clin Infect Dis *32*, 76-102. 10.1086/317537.

1193 43. Snapper, C.M., and Paul, W.E. (1987). Interferon-gamma and B cell stimulatory factor-1
1194 reciprocally regulate Ig isotype production. Science *236*, 944-947.
1195 10.1126/science.3107127.
1196 44. An, Y., Li, S., Jin, X., Han, J.B., Xu, K., Xu, S., Han, Y., Liu, C., Zheng, T., Liu, M., et al. (2022). A
1197 tandem-repeat dimeric RBD protein-based covid-19 vaccine zf2001 protects mice and
1198 nonhuman primates. Emerg Microbes Infect *11*, 1058-1071.
1199 10.1080/22221751.2022.2056524.
1200 45. Tarrés-Freixas, F., Trinité, B., Pons-Grífols, A., Romero-Durana, M., Riveira-Muñoz, E., Ávila-
1201 Nieto, C., Pérez, M., Garcia-Vidal, E., Perez-Zsolt, D., Muñoz-Basagoiti, J., et al. (2022).
1202 Heterogeneous Infectivity and Pathogenesis of SARS-CoV-2 Variants Beta, Delta and
1203 Omicron in Transgenic K18-hACE2 and Wildtype Mice. Front Microbiol *13*, 840757.
1204 10.3389/fmicb.2022.840757.
1205 46. Ying, B., Scheaffer, S.M., Whitener, B., Liang, C.Y., Dmytrenko, O., Mackin, S., Wu, K., Lee,
1206 D., Avena, L.E., Chong, Z., et al. (2022). Boosting with variant-matched or historical mRNA
1207 vaccines protects against Omicron infection in mice. Cell *185*, 1572-1587.e1511.
1208 10.1016/j.cell.2022.03.037.
1209 47. U.S. National Library of Medicine (2021). Safety and Immunogenicity Study of Recombinant
1210 Protein RBD Candidate Vaccine Against SARS-CoV-2 in Adult Healthy Volunteers (COVID-19).
1211 Identifier: NCT05007509. .
1212 48. Cheng, T.M., Blundell, T.L., and Fernandez-Recio, J. (2007). pyDock: electrostatics and
1213 desolvation for effective scoring of rigid-body protein-protein docking. Proteins *68*, 503-
1214 515. 10.1002/prot.21419.
1215 49. Case, D.A., Ben-Shalom, I.Y., Brozell, S.R., Cerutti, D.S., Cheatham III, T.E., Cruzeiro, V.W.D.,
1216 Darden, T.A., Duke, R.E., Ghoreishi, D., Gilson, M.K., et al. (2018). AMBER 2018, University
1217 of California, San Francisco.
1218 50. Jorgensen, W.L., Chandrasekhar, J., Madura, J.D., Impey, R.W., and Klein, M.L. (1983).
1219 Comparison of simple potential functions for simulating liquid water. The Journal of
1220 Chemical Physics *79*, 926-935. 10.1063/1.445869.
1221 51. Maier, J.A., Martinez, C., Kasavajhala, K., Wickstrom, L., Hauser, K.E., and Simmerling, C.
1222 (2015). ff14SB: Improving the Accuracy of Protein Side Chain and Backbone Parameters
1223 from ff99SB. J Chem Theory Comput *11*, 3696-3713. 10.1021/acs.jctc.5b00255.
1224 52. Kollman, P.A., Massova, I., Reyes, C., Kuhn, B., Huo, S., Chong, L., Lee, M., Lee, T., Duan, Y.,
1225 Wang, W., et al. (2000). Calculating structures and free energies of complex molecules:
1226 combining molecular mechanics and continuum models. Acc Chem Res *33*, 889-897.
1227 10.1021/ar000033j.
1228 53. Pettersen, E.F., Goddard, T.D., Huang, C.C., Meng, E.C., Couch, G.S., Croll, T.I., Morris, J.H.,
1229 and Ferrin, T.E. (2021). UCSF ChimeraX: Structure visualization for researchers, educators,
1230 and developers. Protein Sci *30*, 70-82. 10.1002/pro.3943.
1231 54. Pradenas, E., Trinité, B., Urrea, V., Marfil, S., Ávila-Nieto, C., Rodríguez de la Concepción,
1232 M.L., Tarrés-Freixas, F., Pérez-Yanes, S., Rovirosa, C., Ainsua-Enrich, E., et al. (2021). Stable
1233 neutralizing antibody levels 6 months after mild and severe COVID-19 episodes. Med (N Y)
1234 *2*, 313-320.e314. 10.1016/j.medj.2021.01.005.
1235 55. Sánchez-Palomino, S., Massanella, M., Carrillo, J., García, A., García, F., González, N.,
1236 Merino, A., Alcamí, J., Bofill, M., Yuste, E., et al. (2011). A cell-to-cell HIV transfer assay

1237 identifies humoral responses with broad neutralization activity. Vaccine *29*, 5250-5259.
1238 10.1016/j.vaccine.2011.05.016.
1239 56. Brustolin, M., Rodon, J., Rodríguez de la Concepción, M.L., Ávila-Nieto, C., Cantero, G.,
1240 Pérez, M., Te, N., Noguera-Julián, M., Guallar, V., Valencia, A., et al. (2021). Protection
1241 against reinfection with D614- or G614-SARS-CoV-2 isolates in golden Syrian hamster.
1242 Emerg Microbes Infect *10*, 797-809. 10.1080/22221751.2021.1913974.
1243 57. Vidal, E., López-Figueroa, C., Rodon, J., Pérez, M., Brustolin, M., Cantero, G., Guallar, V.,
1244 Izquierdo-Useros, N., Carrillo, J., Blanco, J., et al. (2022). Chronological brain lesions after
1245 SARS-CoV-2 infection in hACE2-transgenic mice. Vet Pathol *59*, 613-626.
1246 10.1177/03009858211066841.

1247

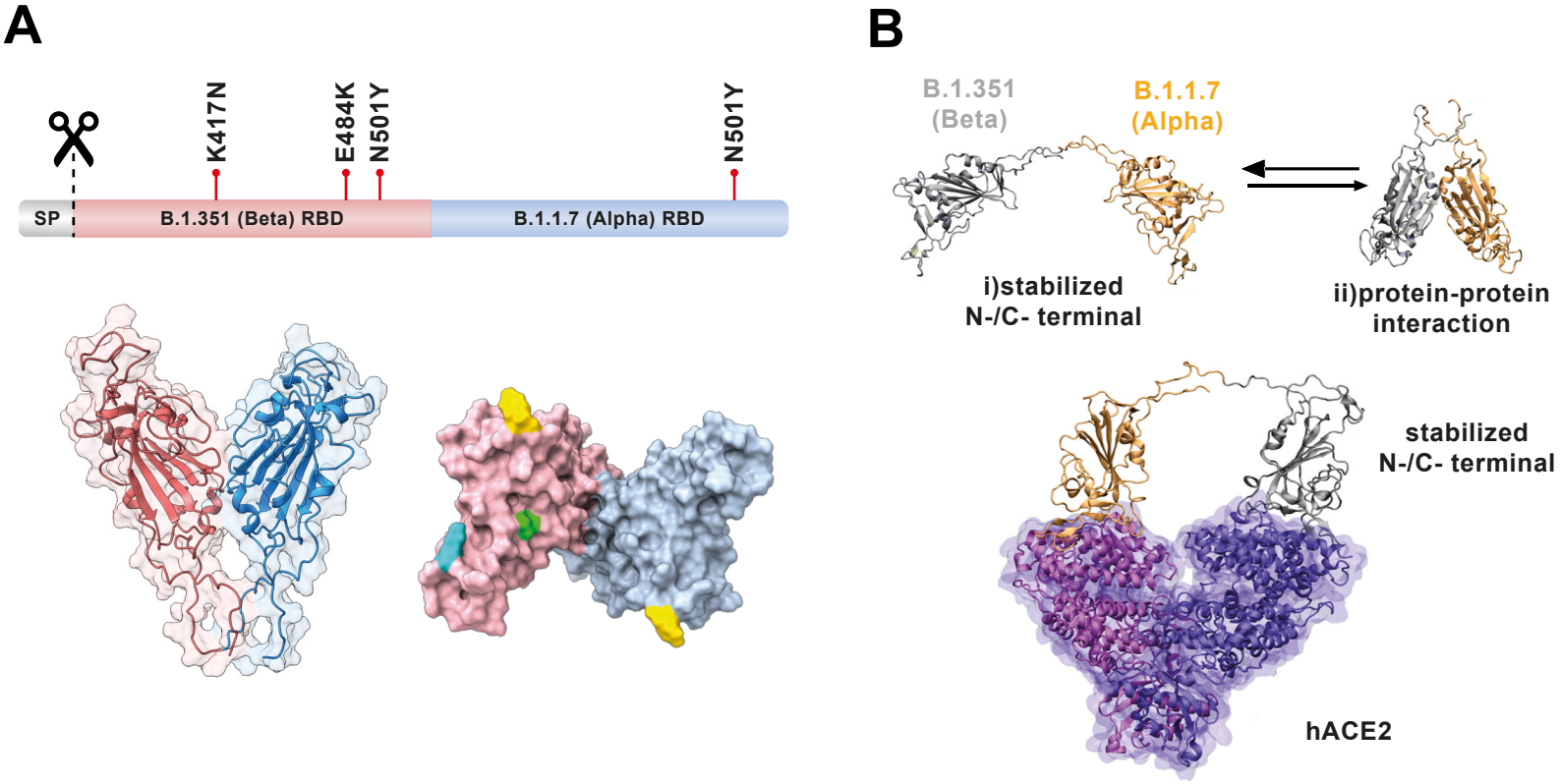

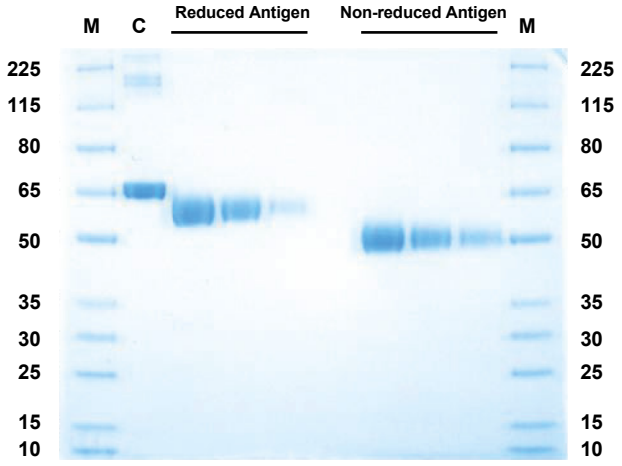

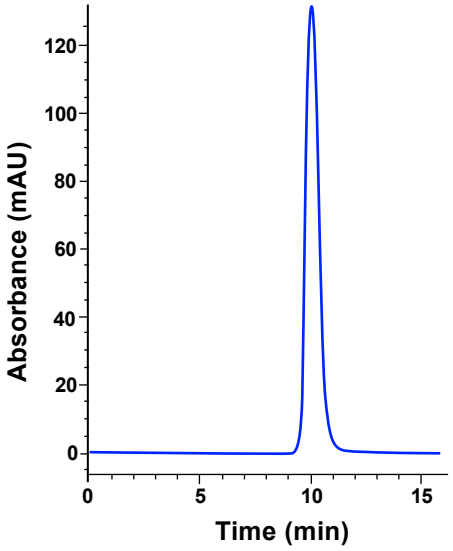

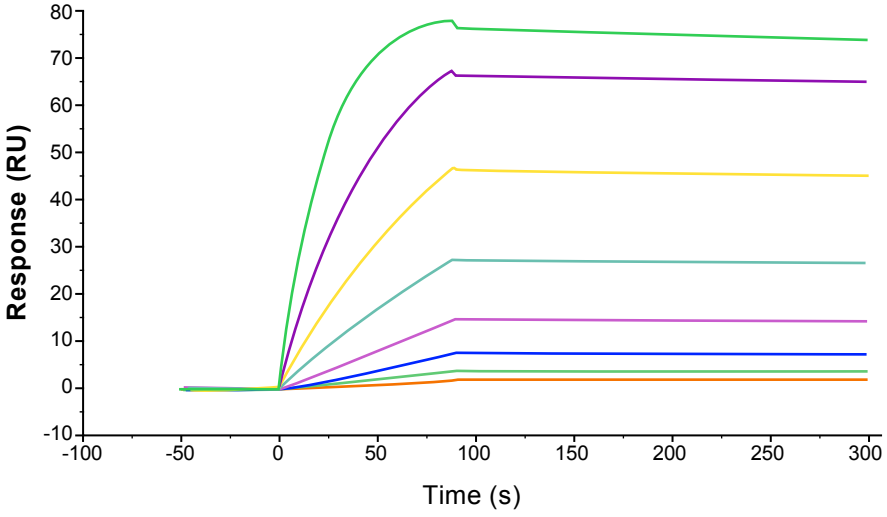

Method	Ligand	K_D(M)
Human IgG (Fc) Capture	Human ACE2 / ACEH Protein, Fc Tag	9.85E-11

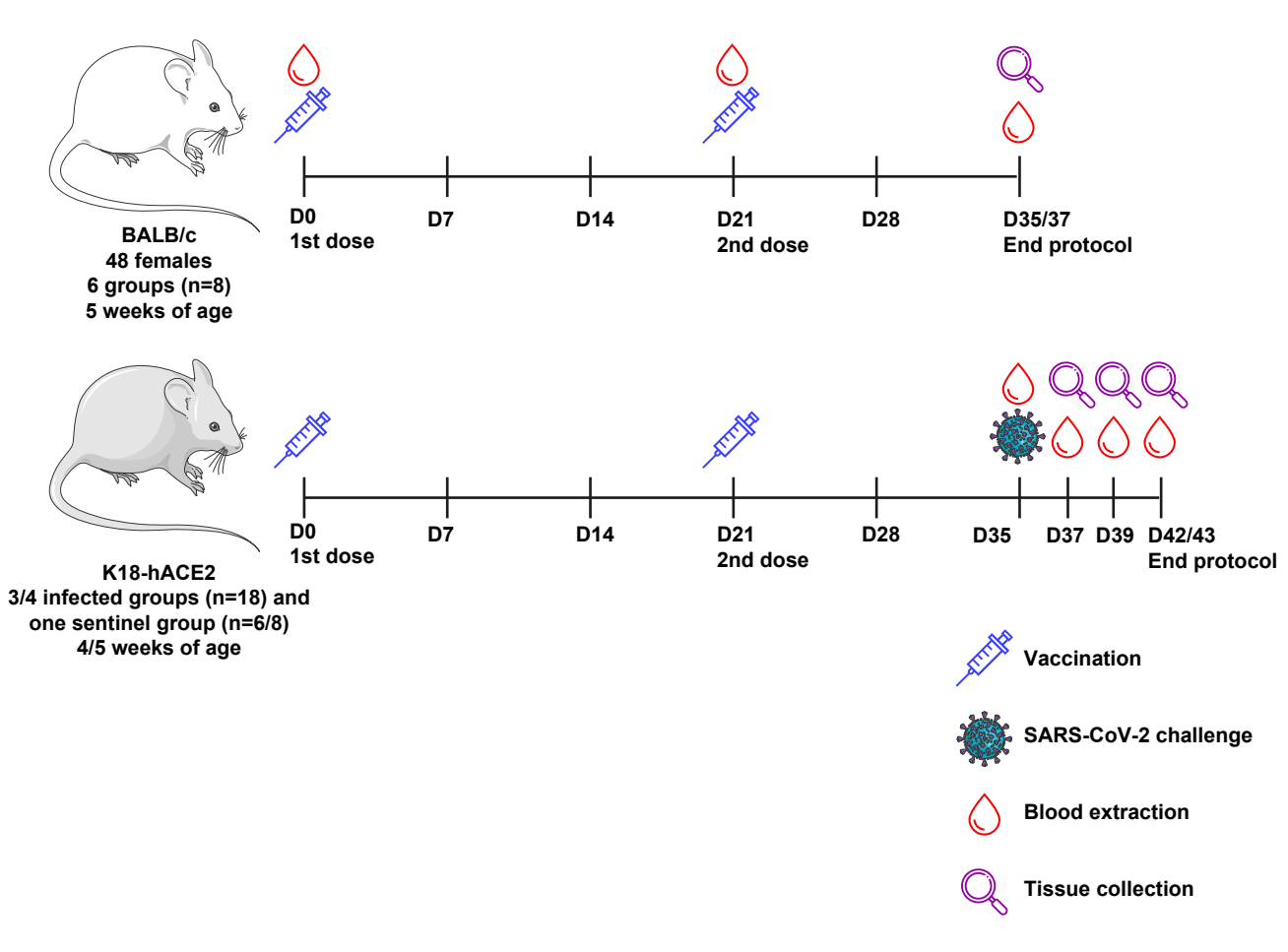
BALB/c
48 females
6 groups (n=8)
5 weeks of age
D0
1st dose
D7
D14
D21
2nd dose
D28
D35/37
End protocol
K18-hACE2
3/4 infected groups (n=18) and
one sentinel group (n=6/8)
4/5 weeks of age
D0
1st dose
D7
D14
D21
2nd dose
D28
D35
D37
D39
D42/43
End protocol
Vaccination
SARS-CoV-2 challenge
Blood extraction
Tissue collection

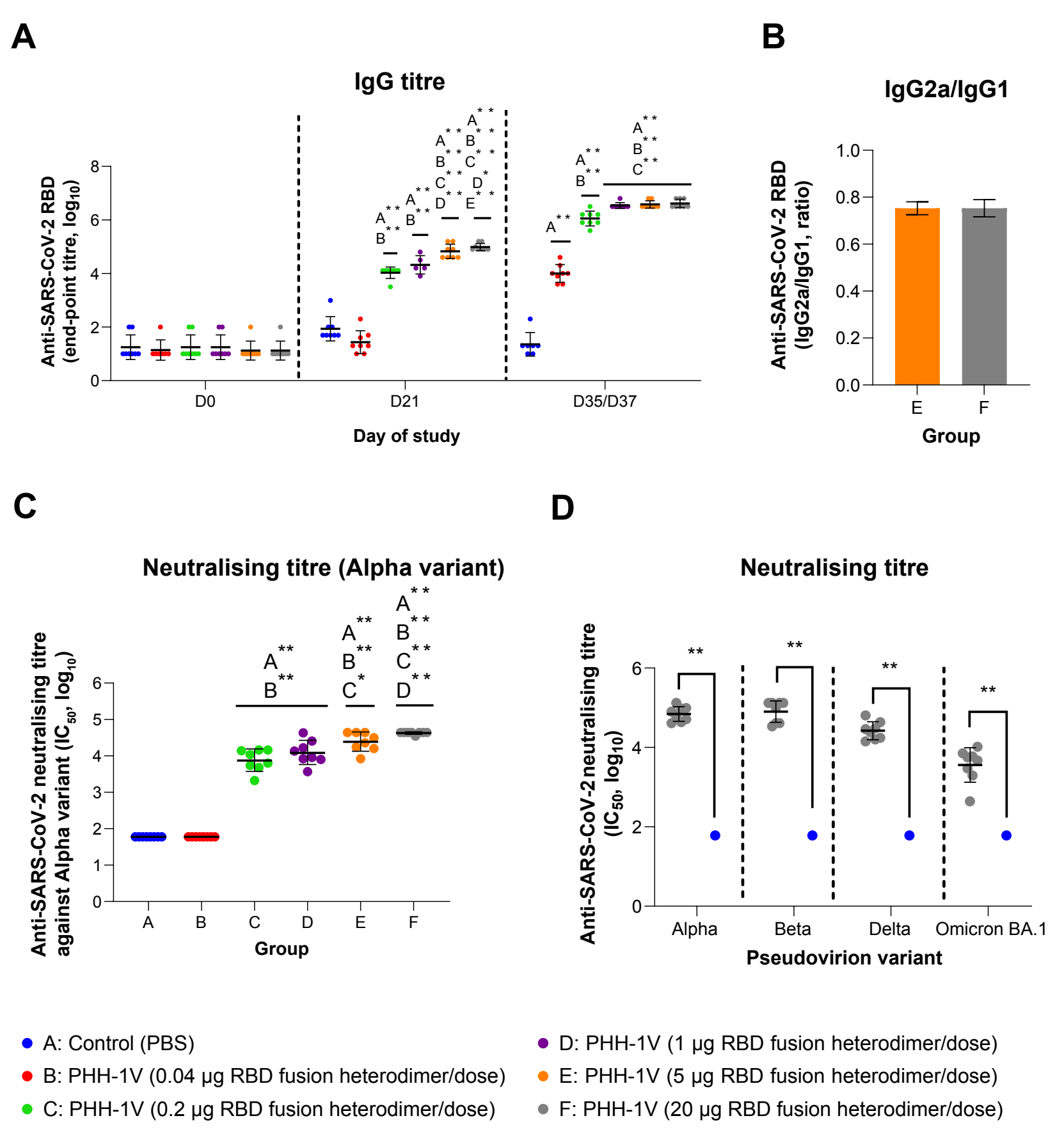
A
IgG titre
Anti-SARS-CoV-2 RBD (end-point titre, log10)
0
2
4
6
8
D0
D21
D35/D37
Day of study
B
IgG2a/IgG1
Anti-SARS-CoV-2 RBD (IgG2a/IgG1, ratio)
0.0
0.2
0.4
0.6
0.8
1.0
E
F
Group
C
Neutralising titre (Alpha variant)
Anti-SARS-CoV-2 neutralising titre against Alpha variant (IC50, log10)
0
1
2
3
4
5
6
A
B
C
D
E
F
Group
D
Neutralising titre
Anti-SARS-CoV-2 neutralising titre (IC50, log10)
0
2
4
6
Alpha
Beta
Delta
Omicron BA.1
Pseudovirion variant
A: Control (PBS)
B: PHH-1V (0.04 µg RBD fusion heterodimer/dose)
C: PHH-1V (0.2 µg RBD fusion heterodimer/dose)
D: PHH-1V (1 µg RBD fusion heterodimer/dose)
E: PHH-1V (5 µg RBD fusion heterodimer/dose)
F: PHH-1V (20 µg RBD fusion heterodimer/dose)

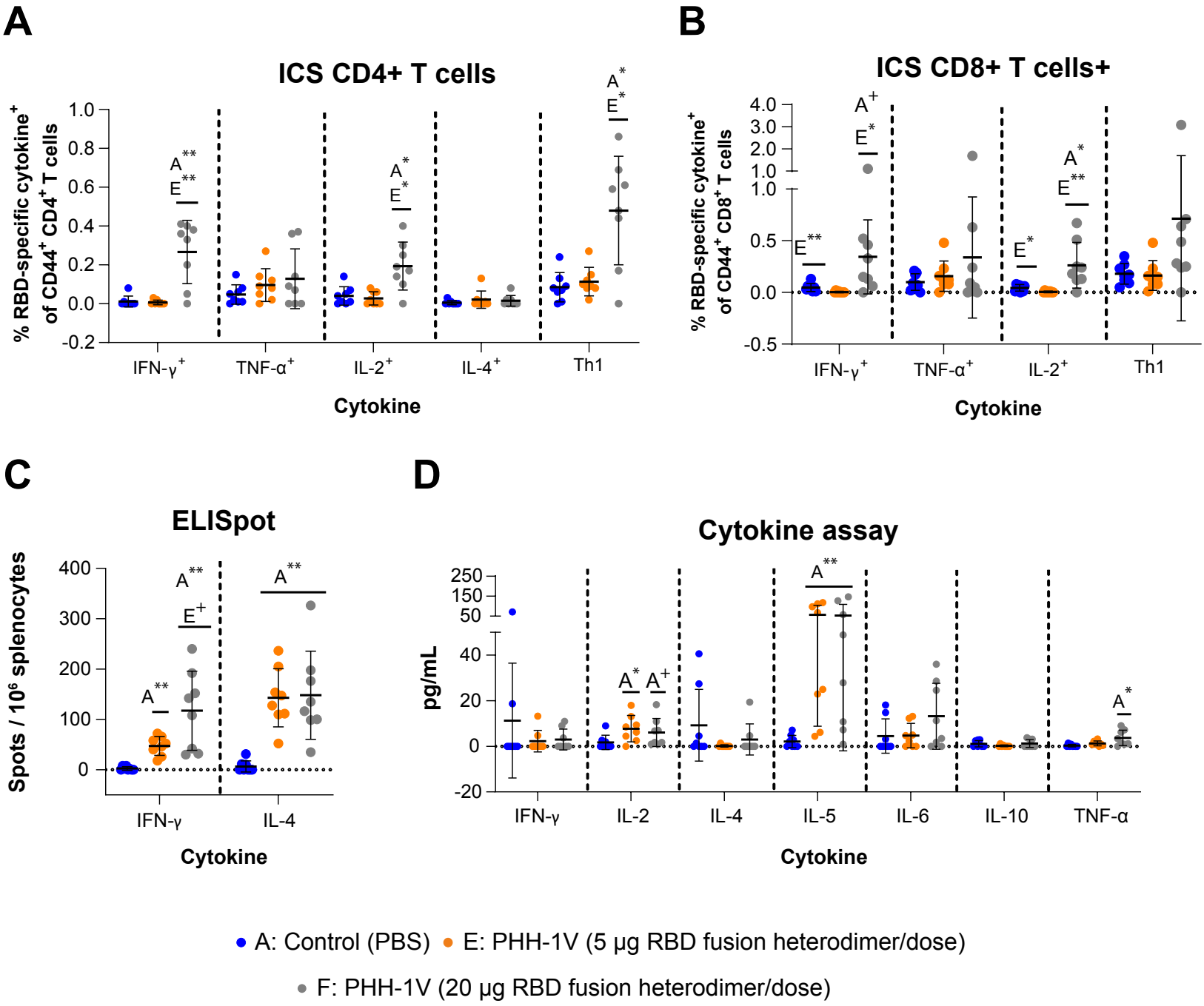
A
ICS CD4+ T cells
% RBD-specific cytokine+ of CD44+ CD4+ T cells
1.0
0.8
0.6
0.4
0.2
0.0
-0.2
A**
E**
A*
E*
A*
E*
IFN-γ+
TNF-α+
IL-2+
IL-4+
Th1
Cytokine
B
ICS CD8+ T cells+
% RBD-specific cytokine+ of CD44+ CD8+ T cells
4.0
3.0
2.0
1.0
1.0
0.5
0.0
-0.5
A+
E*
E**
A*
E**
E*
IFN-γ+
TNF-α+
IL-2+
Th1
Cytokine
C
ELISpot
Spots / 10^6 splenocytes
400
300
200
100
0
A**
E+
A**
A**
IFN-γ
IL-4
Cytokine
D
Cytokine assay
pg/mL
250
150
50
40
20
0
-20
A*
A+
A**
A*
IFN-γ
IL-2
IL-4
IL-5
IL-6
IL-10
TNF-α
Cytokine
A: Control (PBS)
E: PHH-1V (5 µg RBD fusion heterodimer/dose)
F: PHH-1V (20 µg RBD fusion heterodimer/dose)

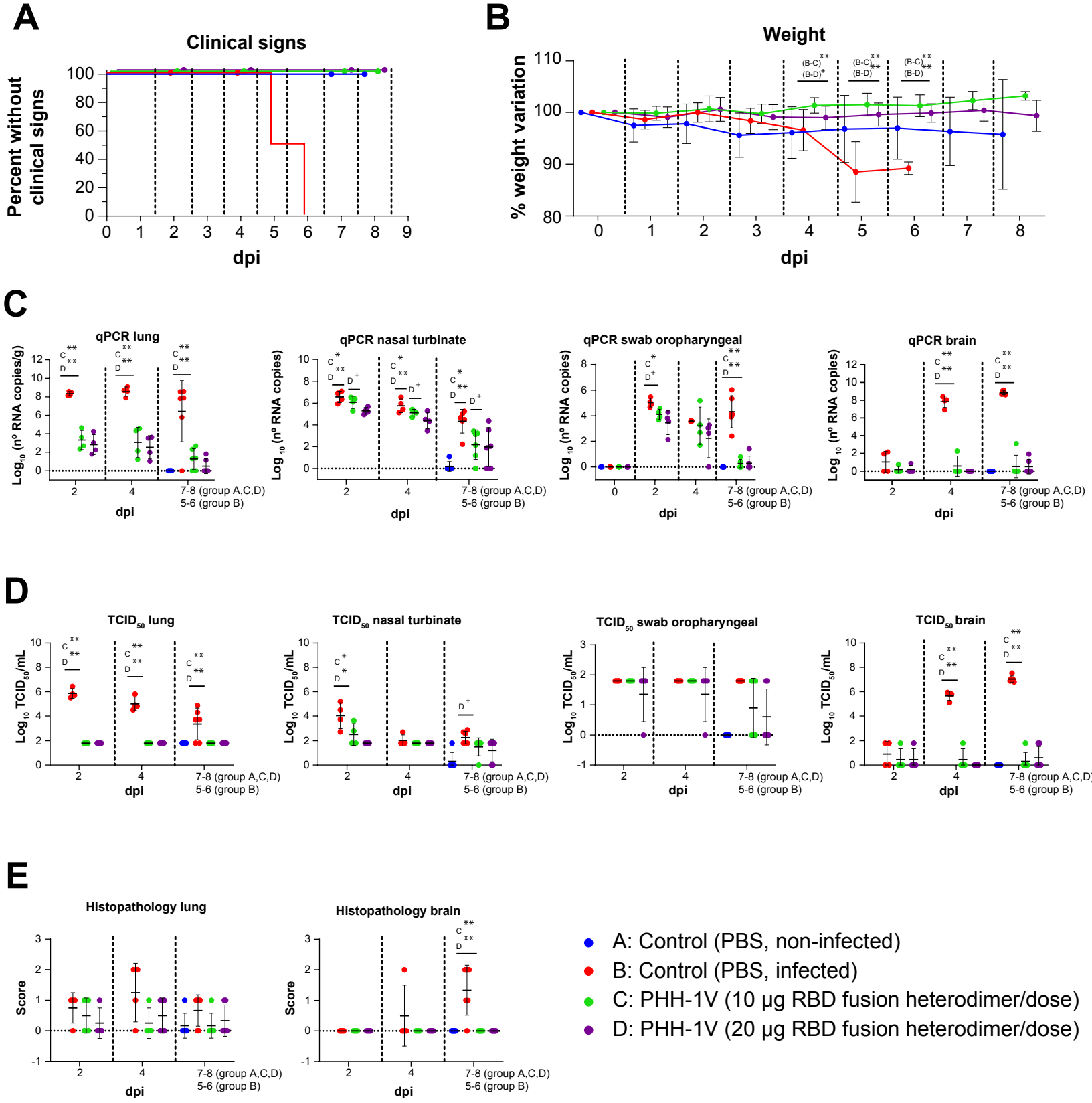
A
Clinical signs
Percent without clinical signs
dpi
B
Weight
% weight variation
dpi
C
qPCR lung
qPCR nasal turbinate
qPCR swab oropharyngeal
qPCR brain
Log10 (nº RNA copies/g)
Log10 (nº RNA copies)
dpi
7-8 (group A,C,D)
5-6 (group B)
D
TCID50 lung
TCID50 nasal turbinate
TCID50 swab oropharyngeal
TCID50 brain
Log10 TCID50/mL
E
Histopathology lung
Histopathology brain
Score
A: Control (PBS, non-infected)
B: Control (PBS, infected)
C: PHH-1V (10 µg RBD fusion heterodimer/dose)
D: PHH-1V (20 µg RBD fusion heterodimer/dose)

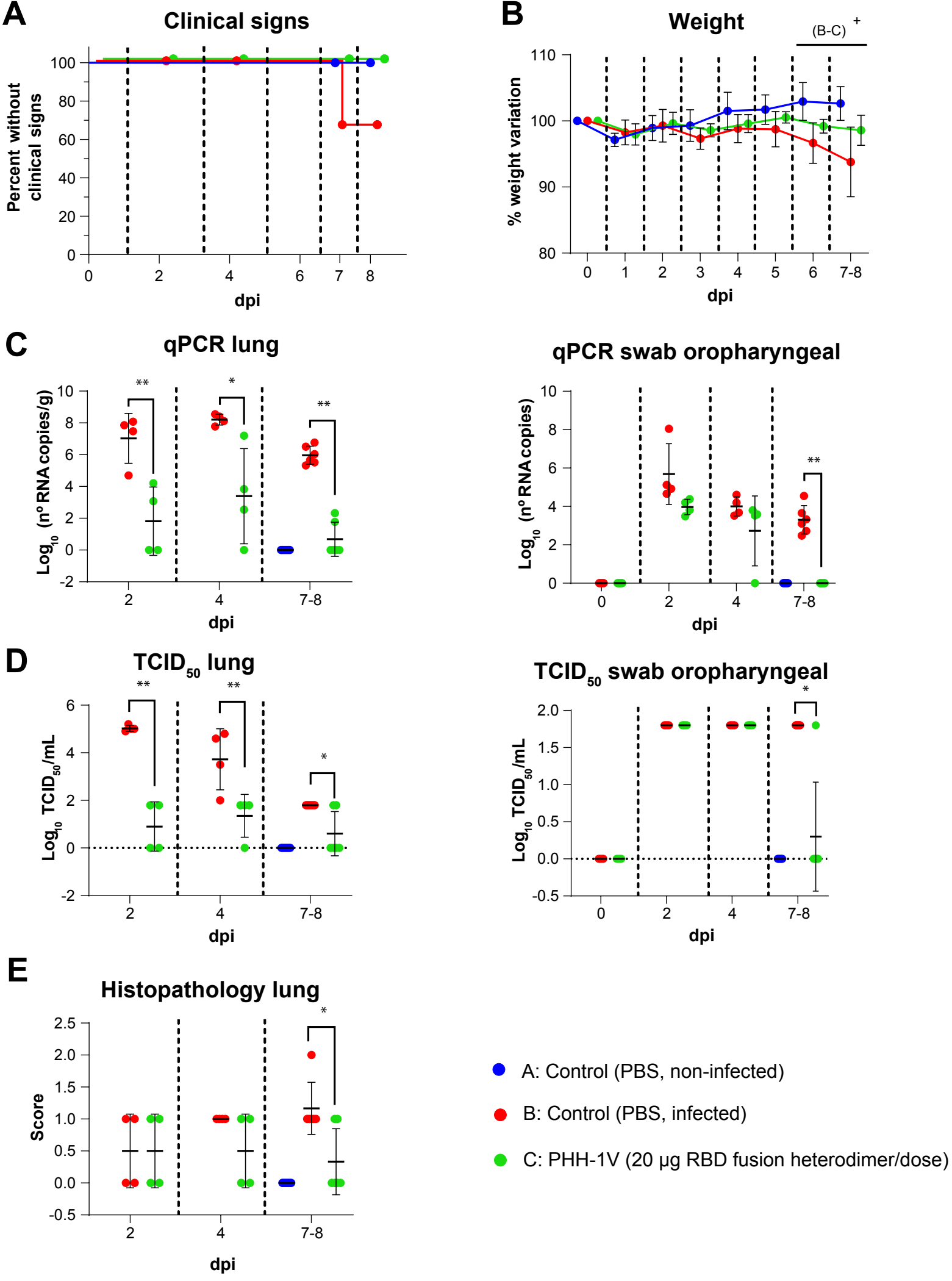
A
Clinical signs
Percent without clinical signs
dpi
B
Weight
(B-C) +
% weight variation
dpi
C
qPCR lung
Log10 (nº RNA copies/g)
dpi
qPCR swab oropharyngeal
Log10 (nº RNA copies)
dpi
D
TCID50 lung
Log10 TCID50/mL
dpi
TCID50 swab oropharyngeal
Log10 TCID50/mL
dpi
E
Histopathology lung
Score
dpi
A: Control (PBS, non-infected)
B: Control (PBS, infected)
C: PHH-1V (20 µg RBD fusion heterodimer/dose)

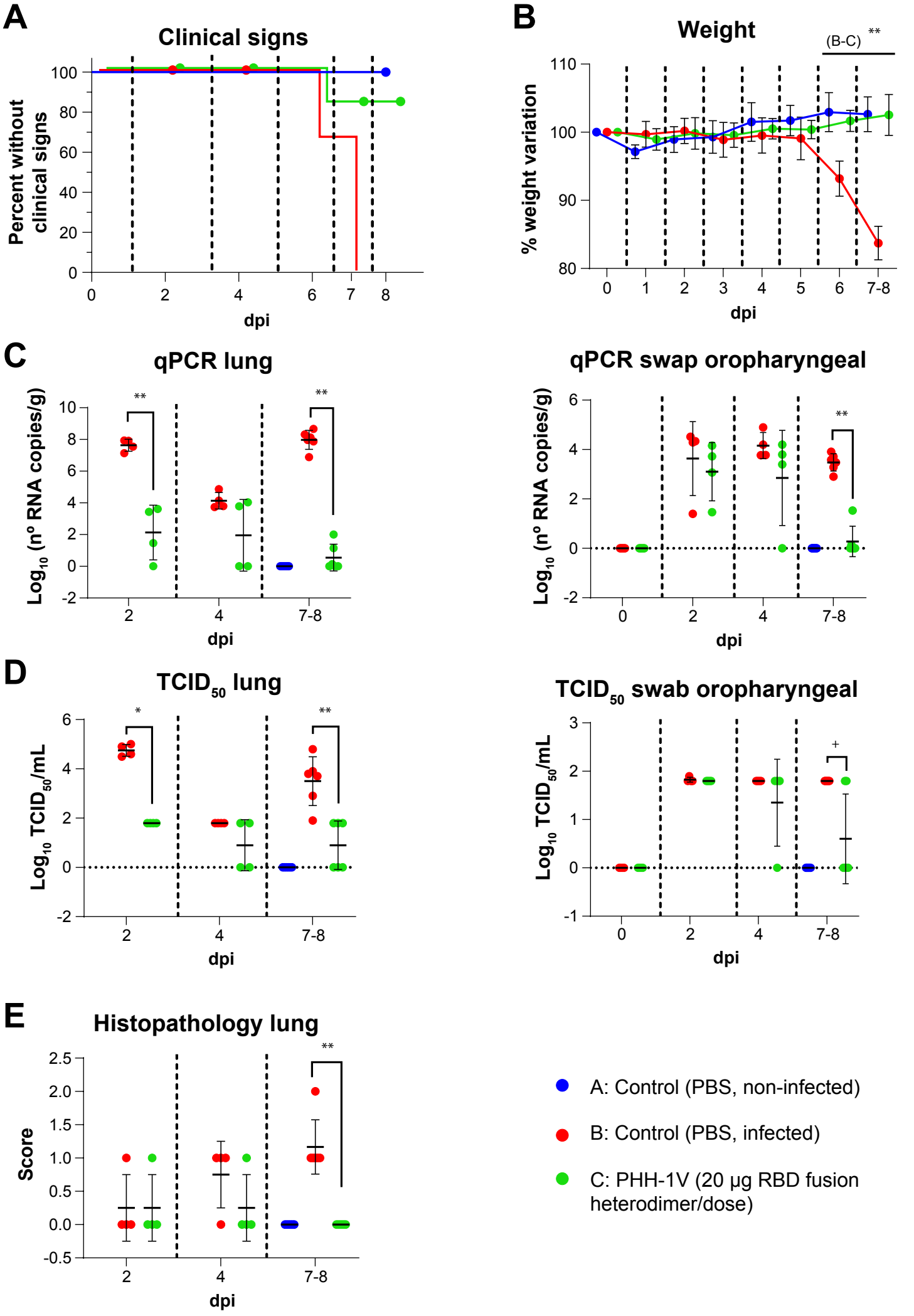
A
Clinical signs
Percent without clinical signs
dpi
B
Weight
(B-C) **
% weight variation
dpi
C
qPCR lung
Log10 (nº RNA copies/g)
dpi
qPCR swap oropharyngeal
Log10 (nº RNA copies/g)
dpi
D
TCID50 lung
Log10 TCID50/mL
dpi
TCID50 swab oropharyngeal
Log10 TCID50/mL
dpi
E
Histopathology lung
Score
dpi
A: Control (PBS, non-infected)
B: Control (PBS, infected)
C: PHH-1V (20 µg RBD fusion heterodimer/dose)

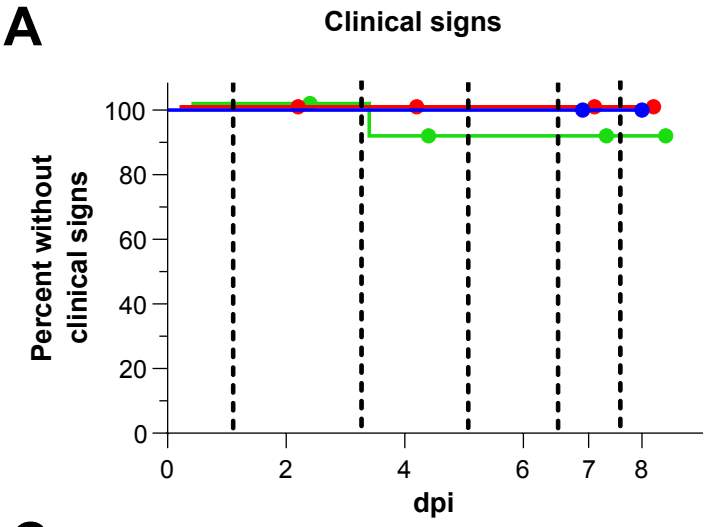

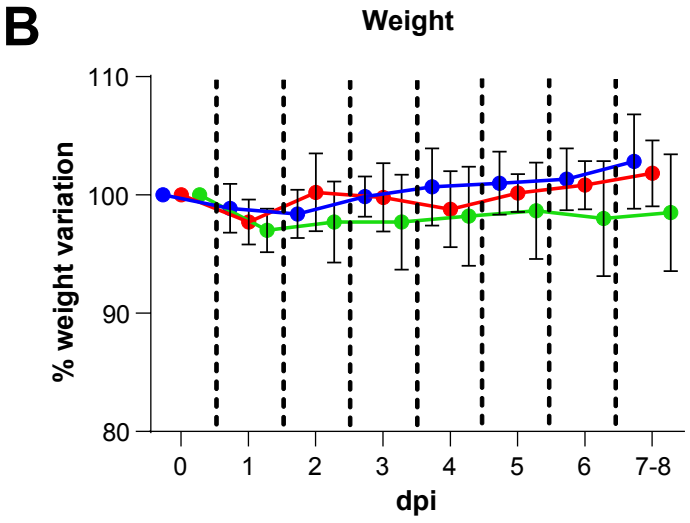

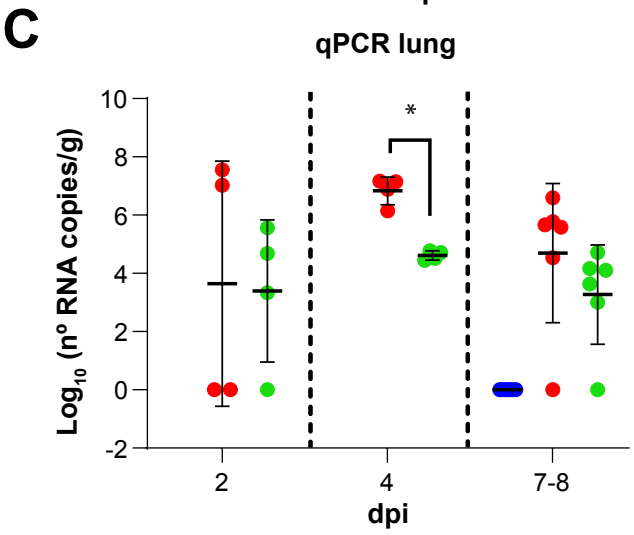

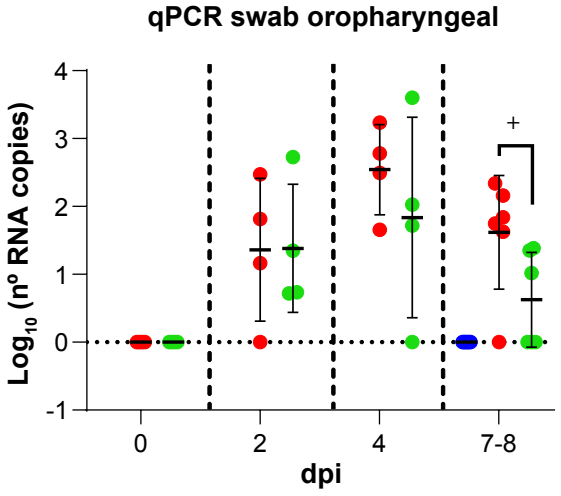

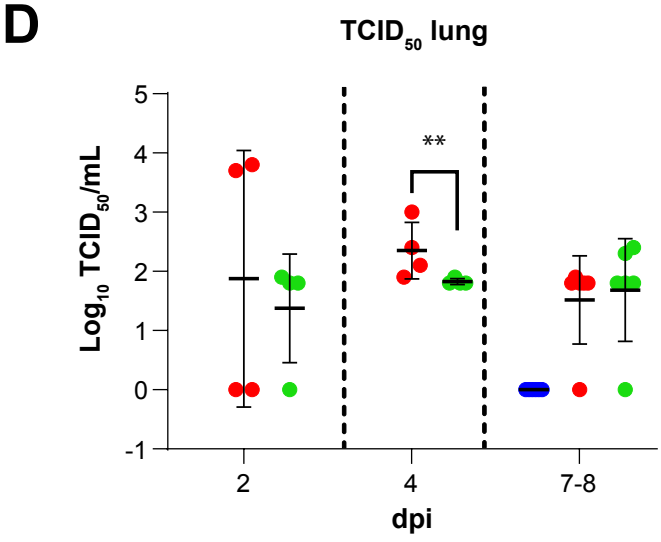

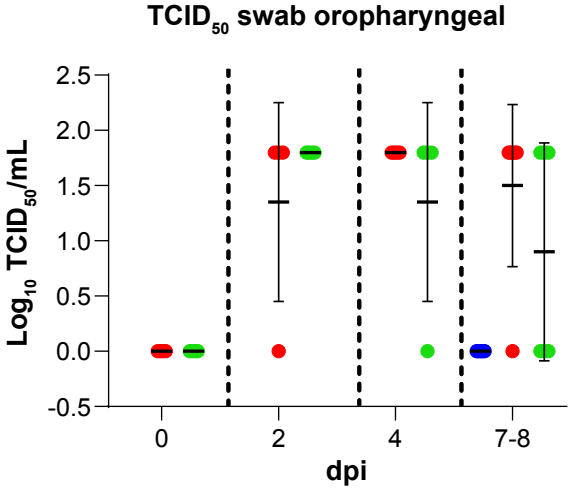

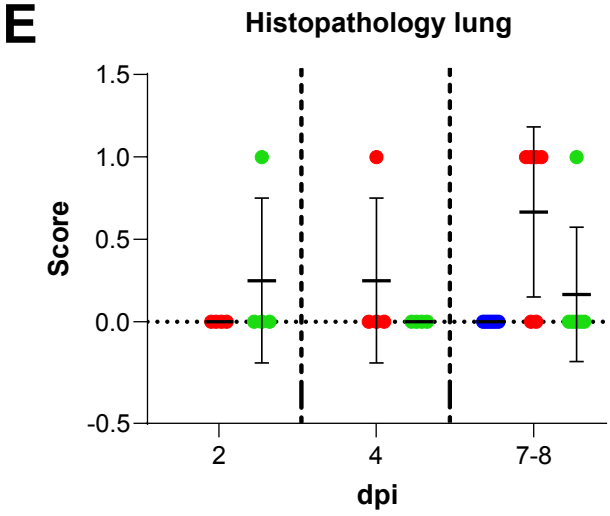

- A: Control (PBS, non-infected)
- B: Control (PBS, infected)
- C: PHH-1V (20 µg RBD fusion heterodimer/dose)